Argonne NATIONAL LABORATORY

Intra-Laboratory Memo

**September 3, 2010**

**TO:** **James E. Matos**

**FROM:** **Earl E. Feldman**

**SUBJECT:** **Steady-State Thermal-Hydraulic Analysis for Forced-Convective Flow in the Rhode Island Nuclear Science Center (RINSC) Reactor**

### 4.6.1 Hydraulic Design

The Rhode Island Nuclear Science Center (RINSC) reactor primary and secondary coolant systems have been updated to provide redundant coolant loops. Although not required for operation at 2 MW, two-loop operation is possible. The nominal measured primary coolant flow rate for operation at 2 MW is 1950 gpm.

The thermal analysis of the LEU core requires that the flow rate in each fueled channel be known. The LEU core has 14 geometrically identical essentially square fuel assemblies. As shown in Figure 4.6-1, the 14 fuel assemblies are arranged in the three rows of assemblies that are between the two sets of control blades. Each assembly has 22 evenly spaced fuel plates that form 21 internal coolant channels. The first and the last fuel plate bound two lateral sides of the assembly. The 22 fuel plates are held in place by two side plates. All 14 fuel assemblies are oriented in the core in the same way so that the fuel plates are parallel to each other and perpendicular to the control blades.

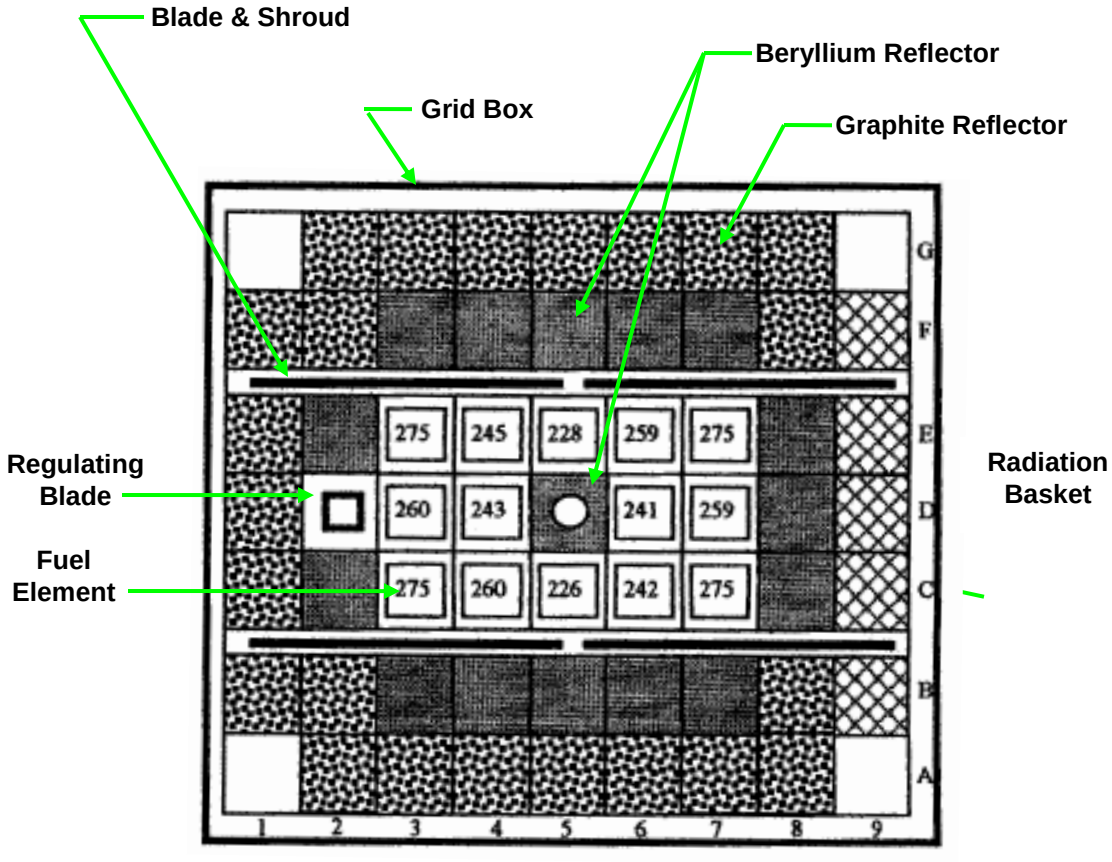


**Figure 4.6-1 LEU Equilibrium Core Layout**

The two adjacent end fuel plates of two adjacent fueled assemblies in the same row form a coolant channel. A coolant channel is also formed where an end fuel plate is adjacent to a

beryllium reflector or next to the regulating blade, which is the assembly immediately adjacent to the left of the middle row of fuel assemblies in the figure. Thus, there are four types of fueled channels to be considered – 1) a channel that is between two adjacent fuel plates within the same assembly, 2) a channel formed by two adjacent end fuel plates that belong to two immediately adjacent fuel assemblies, and 3) a channel formed between an end fuel plate of a fuel assembly and a beryllium reflector, and 4) a channel formed between an end fuel plate of a fuel assembly and the regulating rod.

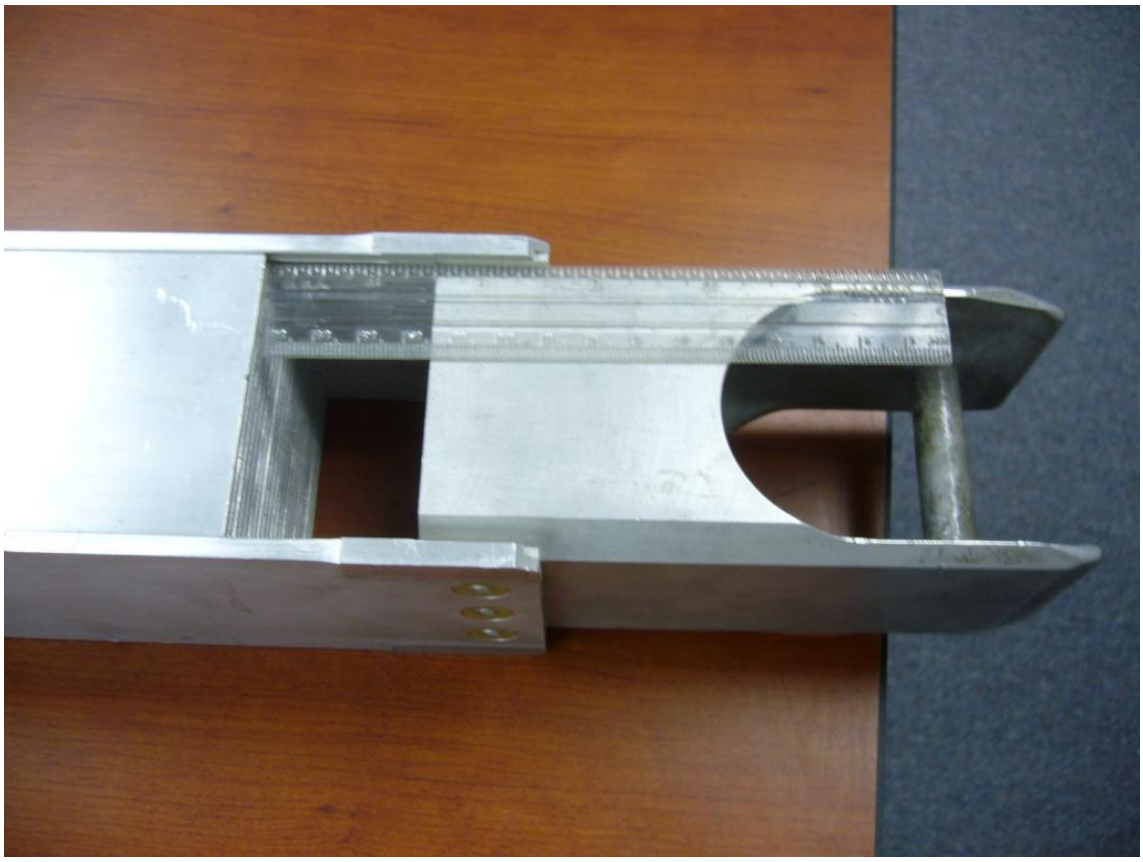

**Figure 4.6-2 – End of Fuel Assembly**
**(Ends of side plates, shown on left, attached to end box, shown on right. 6-inch plastic ruler is included to show scale.)**

Each fuel assembly has a square end box, which serves as a lower adapter, or flow nozzle, for the assembly. The end box is inserted into a square hole in the grid plate. This arrangement holds the assembly in place. The two side plates of a fueled assembly connect to two opposite sides of the end box, as shown in Figure 4.6-2. There is about a 1-inch overlap between the bottom end of the side plates and the top of the end box to allow the two side plates of each assembly to be rigidly fastened to its end box. The bottom edges of the side plates rest on the top of the grid plate. Thus, the top of the end box is about 1-inch above the top of the grid plate. The 22 parallel fuel plates connect only to the two side plates and not to the end box. When the assembly is fully inserted into the grid plate there is about a 2.5-inch clearance between the top of the grid plate and the bottom edge of the fuel plates. Thus, the flow down the channel formed

between two adjacent end plates can go under the bottom edges of the end plates, enter the end box, and merge with the flow streams that came from inside the assemblies. The pump draws all of these streams into the outlet plenum, which is below the grid plate.

The total flow rate through the primary pump is measured and controlled. This total flow includes not only flow past fuel plates, but also flow through the reflectors, flow through the control rod blades, and several other non-fueled paths within the core box. The total flow also includes the flow through the gamma shield, which is connected in parallel with the core box.

### 4.6.2 Hydraulic Modeling Strategy

Page 53 of the General Electric Safeguards Report[1] provides the volumetric flow rates in gpm shown in Table 4.6-1. This data shows that 90.33% of the primary flow through the reactor core box for the HEU core went to cool the fuel elements and the remaining other 9.67% went through other paths within the core box. The flow fractions shown in the table are not applicable to the LEU core because the hydraulic resistance for the LEU core is much greater than that for the HEU core. Although the flow area for an HEU assembly is almost the same at that for an LEU assembly, the HEU core had 30 fueled assemblies and LEU core has only 14 fueled assemblies. In addition, the larger number of fuel plates per assembly for the LEU core – 22 for the LEU versus 18 for the HEU – causes the LEU assembly to have a smaller hydraulic diameter and more hydraulic resistance than does an HEU assembly. The smaller hydraulic resistance for the HEU core causes a larger fraction of the total flow to go through the fueled channels and a smaller fraction to go through all of the remaining paths.

**Table 4.6-1 – HEU Flow Distribution**

| Item | Value | |
|---|---|---|
| | gpm | % |
| Fuel Elements | 1355 | 90.33 |
| Control Blades | 45 | 3.00 |
| Graphite Reflectors | 47 | 3.13 |
| Radiation Basket | 10 | 0.67 |
| Neutron Source | 3 | 0.20 |
| Leakage | 40 | 2.67 |
| Total | 1500 | 100.0 |

The flow rates in Table 4.6-1 can be indirectly used to calibrate a hydraulics model for the LEU core because many of the flow paths in the LEU are the same as those in the HEU core. This calibration requires that the hydraulics of the HEU core be modeled. The 30 fuel assemblies in the HEU core are arranged in a rectangular array of five rows of six assemblies. Three of the parallel rows are between the two sets of control blades and the other two are on either side. There are no beryllium reflectors in the HEU core. The number of graphite reflectors is the same in the HEU core as in the LEU core. The equilibrium LEU core was formed by replacing 30 HEU assemblies with 14 LEU assemblies and 16 beryllium reflectors. Also, the regulating rod and three of the graphite reflectors were relocated within the core. The HEU core had the same four types of fuel channels except that the channels formed between end fuel plates and beryllium reflectors are formed between end fuel plates and graphite reflectors.

The HEU core will be modeled first. This model will contain five types of parallel flow paths – the four fueled types of fuel paths and a fifth flow path that represents all of the non-fueled flow paths in the core box taken together. The analysis of the HEU core will allow the resistance in the fifth path to be characterized so that it can be quantified in a hydraulics model for the LEU

core. For the HEU core the inlet-to-outlet pressure drop across all of the parallel paths, ΔP, would be the same since all originate at a common source and end at a common sink. Explicit details describing the four fueled types of paths will be included in the model. For the fifth type of path, which is represented as a single path, the model will simply assume the pressure drop across the path, which is the common pressure drop, is proportional to the combined flow rate through all of the paths of this type, $\dot{m}_{NON-FUEL}$, raise to the α power, or:

$$\Delta P = C_1 \, (\dot{m}_{NON-FUEL})^{\alpha} \tag{1}$$

where $C_1$ is a proportionality constant. For fully turbulent flow α is between 1.75 and 2.0. Since the non-fueled flow paths in the reactor are dominated by friction, as represented by a friction factor, a value of 1.8 would be a reasonably accurate value and will be assumed in the analysis. As will be shown, $C_1$ can be deduced from the model with the aid of the HEU flow data in Table 4.6-1. This model will also yield the flow rates in each of the fueled paths of the HEU core although these flow rates are not needed for the current analysis. A similar model will be developed for the LEU core. The non-fueled paths for the LEU core that are the same as in the HEU core will be represented by equation (1) with $C_1$ as deduced from the analysis of the HEU core.

The 16 beryllium reflectors introduce additional non-fueled flow paths within the core that will be included in the LEU hydraulics model. Except for the central beryllium reflector, all of these reflectors have a 0.25-inch diameter vertical coolant hole through the middle of the reflector. The central reflector is designed to hold irradiation test samples and has a plug that restricts flow when it is otherwise empty. In either case the magnitude of the flow through it should be no greater than that of the other beryllium reflectors, which is about 0.05% of the total reactor flow. Therefore, the central beryllium reflector will be modeled as if it were the same as the other 15. There are also 10 flow paths between adjacent beryllium reflectors – four in the top row of beryllium reflectors, four in the bottom row, and two among the three beryllium reflectors on the right side between the control blades. Two more flow paths are formed between each of two the beryllium reflectors that are on two opposing sides of the regulating blade and the regulating blade itself. Once the flow rate in each of the LEU fueled channel is known, the thermally most limiting channel can be identified and its behavior can be studied.

### 4.6.3 Hydraulic Parameters

Key parameters for the LEU and HEU core are summarized in Table 4.6-2 and are discussed below. A way to determine the channel width inside a fueled assembly is a follows. The nominal width of the LEU fuel plate is 2.790 inches. Each LEU fuel assembly has 22 fuel plates and two side plates. Each side plate in an LEU assembly has 22 grooves that are 0.094 inches deep. The fuel plates are swaged into the grooves of the two side plates. The channel width is the plate width reduced by two groove depths, or 2.790 inches − 2 × 0.094 inches = 2.602 inches. Another way to determine this channel width is as follows. A drawing of the LEU assembly shows the outer dimension from side plate to side plate to be 2.995 inches. This dimension diminished by the thickness of two 0.187-inch thick side plates, yields a fuel channel width of 2.621 inches. The slightly larger value here may be to allow for tolerances in the fuel plate width. The channel width will be taken to be 2.62 inches. The total length of the plate is 25

inches. These dimensions will be assumed to apply for the HEU fuel as well since small differences in these dimensions are not significant.

**Table 4.6-2 – Key Hydraulics Parameters**

| Item | LEU | HEU |
|---|---|---|
| Number of plates | 22 | 18 |
| Channel Width, inches | 2.62 | 2.62 |
| Plate Length, inches | 25 | 25 |
| Heated Length, inches | 24 | 24 |
| Number of Fueled Channels × Channel Thickness, inches* | | |
| Internal | 294 × 0.088 | 510 × 0.107 |
| End – Between Fuel Assemblies | 10 × 0.112 | 25 × 0.161 |
| End – Next to Graphite Reflector | | 9 × 0.087 |
| End – Next to Beryllium Reflector | 7 × 0.0645 | |
| End – Next to Regulating Rod | 1 × 0.1035 | 1 × 0.128 |
| Number of Channels between Beryllium Reflectors × Channel Thickness, inches* | 10 × 0.017 | |

***For the channels that are formed on one or both sides by a reflector, the channel thickness ignores the recessed regions. However, in the hydraulic analysis, corrections to the flow areas and the wetted perimeters were made to account for the recessed regions.**

The channel thickness within a fuel assembly is determined as follows. The side-plate drawings for both the HEU and LEU cores provide the pitch from one groove to the next – 0.167 inches for the HEU core and 0.138 inches for the LEU core. The coolant channel spacing within each assembly is this groove pitch minus the plate thickness. The plate thickness is 0.050 inches for the LEU fuel and 0.060 inches for the HEU fuel. Based on this data the LEU channel spacing is 0.138 − 0.050, or 0.088 inches and the HEU channel spacing is 0.167 − 0.060, or 0.107 inches. A drawing of the LEU fuel assembly shows that the channel thickness is between 0.082 and 0.094 inches, or 0.088±0.006 inches. Drawing 192C551 of the HEU fuel assembly shows that the channel thickness is 0.107±0.010 inches.

The reactor grid plate design drawing shows that all fueled assemblies and reflectors for both the LEU and the HEU core are on a 3.060-inch square pitch. In determining the sizes of gaps between an assembly, reflector, or regulating rod and its immediate neighbor, one can think of each assembly, reflector, or regulating rod as being centered in an imaginary 3.060-inch square unit cell. The LEU assembly has 22 fuel plates. The channel thickness between the end channels of two immediately adjacent LEU assemblies is 3.060 inches − (22 × 0.050 + 21 × 0.088) inches = 0.112 inches. The HEU core has 18 plates per assembly. The channel thickness between the end channels of two immediately adjacent HEU assemblies is the 3.060 inches − (18 × 0.060 + 17 × 0.107) inches = 0.161 inches. The number of each of these channel types is easy to count and is as shown in Table 4.6-2 along with the numbers of each of the other channel types.

The four sides of each square beryllium or graphite reflector are not flat. Instead the last 0.625 inches before each corner is raised relative to the rest of the face, which is about 1.8 inches wide. Apparently, these raised spots are provided to minimize the lateral friction during insertion and removal of assemblies and reflectors and also possibly to better constrain the position of each reflector relative to its neighboring reflectors.

The beryllium reflector is 3.041 to 3.045 inches on a side, including the raised corners. These corners are raised 0.019 to 0.025 inches relative to the rest of each lateral face. Alternatively, the part of the width between the corners can be considered to be recessed. In determining the channel spacing between the beryllium reflector and the adjacent end plate, we will consider the reflector to be a square that is 3.043 inches on a side. Thus, the distance from the surface of the beryllium reflector to the boundary of its unit cell is (3.060 − 3.043)/2 inches = 0.0085 inches. The distance from the outer edge of the nearest LEU end fuel plate to the boundary of its unit cell is 0.112/2 inches = 0.056 inches. Thus, the channel thickness between the beryllium reflector and the LEU end fuel plate is 0.0085 + 0.056 inches = 0.0645 inches. The channel thickness between two adjacent beryllium reflectors is 2 × 0.0085 inches = 0.017 inches.

The graphite reflector is 3.047 +0.000 −0.003 inches on a side, including the raised corners. It will be considered to be a square that is 3.047 inches on a side. Thus, the distance from the surface of the graphite reflector to the boundary of its unit cell is (3.060 − 3.047)/2 inches = 0.0065 inches. The distance from the outer edge of the nearest HEU end fuel plate to the boundary of its unit cell is 0.161/2 inches = 0.0805 inches. Thus, the channel thickness between the graphite reflector and the HEU end fuel plate is 0.0065 + 0.0805 inches = 0.087 inches.
In the hydraulic analysis, corrections to the flow areas and the wetted perimeters of channels that have a reflector on one or both sides were made to account for the recessed regions in the graphite and beryllium reflectors. The available drawing for the graphite reflector shows a recessed regions but the value of the depth could not be found. Therefore, the depth was taken to be between 0.019 and 0.025 inches as in the beryllium reflector. The average was used for both reflector types.

The outer dimension of the square regulating rod is 2.965 inches. Thus, the distance from the regulating rod to the boundary of its 3.060-inch unit cell is (3.060 − 2.965)/2 inches = 0.0475 inches. Hence, the thickness of the channel between the regulating rod and the adjacent LEU end plate is 0.0475 + 0.056 inches = 0.1035 inches. The thickness of the channel between the regulating rod and the adjacent HEU end plate is 0.0475 + 0.0805 inches = 0.128 inches.

The end boxes of the beryllium and graphite reflectors are round rather than square. Near the top of each of these end boxes are eight radial horizontal round holes that are equally spaced along the circumference of the end box and at the same elevation. These holes are 0.281 inches in diameter in the beryllium reflector end boxes and provide flow paths from the outside of the reflector through the thickness of the end box wall to the outlet plenum. For the side of the reflector that is next to an end fuel plate these holes would have little effect because the flow can go under the bottom edge of the fuel plate and into the end box of the fuel assembly.

Each of the 14 LEU assemblies has 21 internal channels. Thus, there are 14 × 21 = 294 LEU internal coolant channels. Similarly, there are 510 HEU internal coolant channels because each of the 30 HEU assemblies has 17. The width of all rectangular channels will be taken to be 2.62 inches, which is the width of the LEU internal fueled channel.

### 4.6.4 Hydraulic Modeling Methodology

The HEU and the LEU cores will each be modeled as a series of parallel hydraulic paths, Figures 4.6-3 and 4.6-4. A common source pressure exists at the top of the assemblies and a common sink pressure exists in the outlet plenum. Differences in the velocity of the coolant between the source and sink regions are assume to be small and will be ignored. The gamma shield hydraulics will be assumed to have the same inlet and outlet pressures as is assumed for the fuel assemblies. The inlet to the gamma shield is connected to the core inlet pipe. The outlet to the gamma shield is connected to the core outlet pipe. However, the flow through the gamma shield is not part of the total 1500 gpm in Table 4.6-1 and therefore is not included in the $\dot{m}_{NON-FUEL}$ that is in equation 1.

In general, the pressure drop, $\Delta P$, across any hydraulic path can be represented by:

$$\Delta P = \left( K + f \frac{L}{D} \right) \frac{\rho V^2}{2} = \left( K + f \frac{L}{D} \right) \frac{\dot{m}^2}{2 \rho A^2} \qquad (2)$$

where K represents all of the hydraulic form losses associated with the path, L is the length of the path, D is the hydraulic diameter of the path, f is the Moody friction factor, $\rho$ is the coolant density, $\dot{m}$ is the flow rate, and A is the flow area. Each path from the top of the assemblies to the outlet plenum that passes through a fueled channel will be treated as two shorter paths in series. One shorter path will be along the fuel plates and a second one will be through the nearest end box to the outlet plenum. The total pressure drop for both will be the sum of the pressure drops for the two shorter paths. The flow rate, of course, is the same for both parts of the path.

The velocity through the second part of the path will be obtained by assuming that the flow that enters each square 3.060-inch imaginary unit cell for each fueled assembly stays within its unit cell for the entire trip into the outlet plenum. The flow area of the unit cell above the fuel plates is $3.060^2$ inches$^2$ = 9.364 inches$^2$. This flow area will be used for the assembly flow area in the unit cell everywhere except along the fuel plates and in the end box, including in the outlet plenum. The flow area between the fuel plates is taken to be the channel width, 2.62 inches, times the sum of all channel thickness with the 3.060-inches unit cell. For the HEU core, this value is $2.62 \times (3.060 - 18 \times 0.060)$ inches = 5.19 inches$^2$. For the LEU core, it is $2.62 \times (3.060 - 22 \times 0.050)$ inches = 5.14 inches$^2$. The flow area in the end box can be calculated from drawing 693C864, which shows the flow area to be that of a square between 2.210 and 2.238 inches on a side with round corner of radius of 0.24 to 0.26 inches. Thus, for average dimensions, this area is $(2.224^2 - (1 - \pi/4) \times 0.50^2)$ inches$^2$ = 4.89 inches$^2$. Hence, the velocity of the coolant passing through the end box will the 5.19/4.89 = 1.06 times that exiting the fueled channels in the HEU core and 5.14/4.89 = 1.05 times that exiting the fueled channels in the LEU core.

The first four parallel paths in Figure 4.6-3 represent the four types of fueled paths in the HEU core. Accordingly, each has two resistances in series – one along the fuel plates and a second one through the end boxes. The fifth path in Figure 4.6-3 represents the non-fueled HEU path that carries all of the bypass flow in the HEU core box. The constant $C_1$ in equation 1 pertains to this path. The first path shown in Figure 4.6-3 represents 510 identical parallel paths, each with

the flow rate of one internal fueled coolant channel inside a typical HEU assembly. Similarly, the second path shown represents 25 identical paths, the third represents 9, and the fourth and the fifth each represent only one in the model. In the reactor the fifth path actually represents many parallel paths combined. Keeping track of how many identical paths each path in the model represents is important in summing up all of the flows from all of the parallel paths in the network to obtain the total flow rate for the network. This total must equal the specified total through the HEU core box.

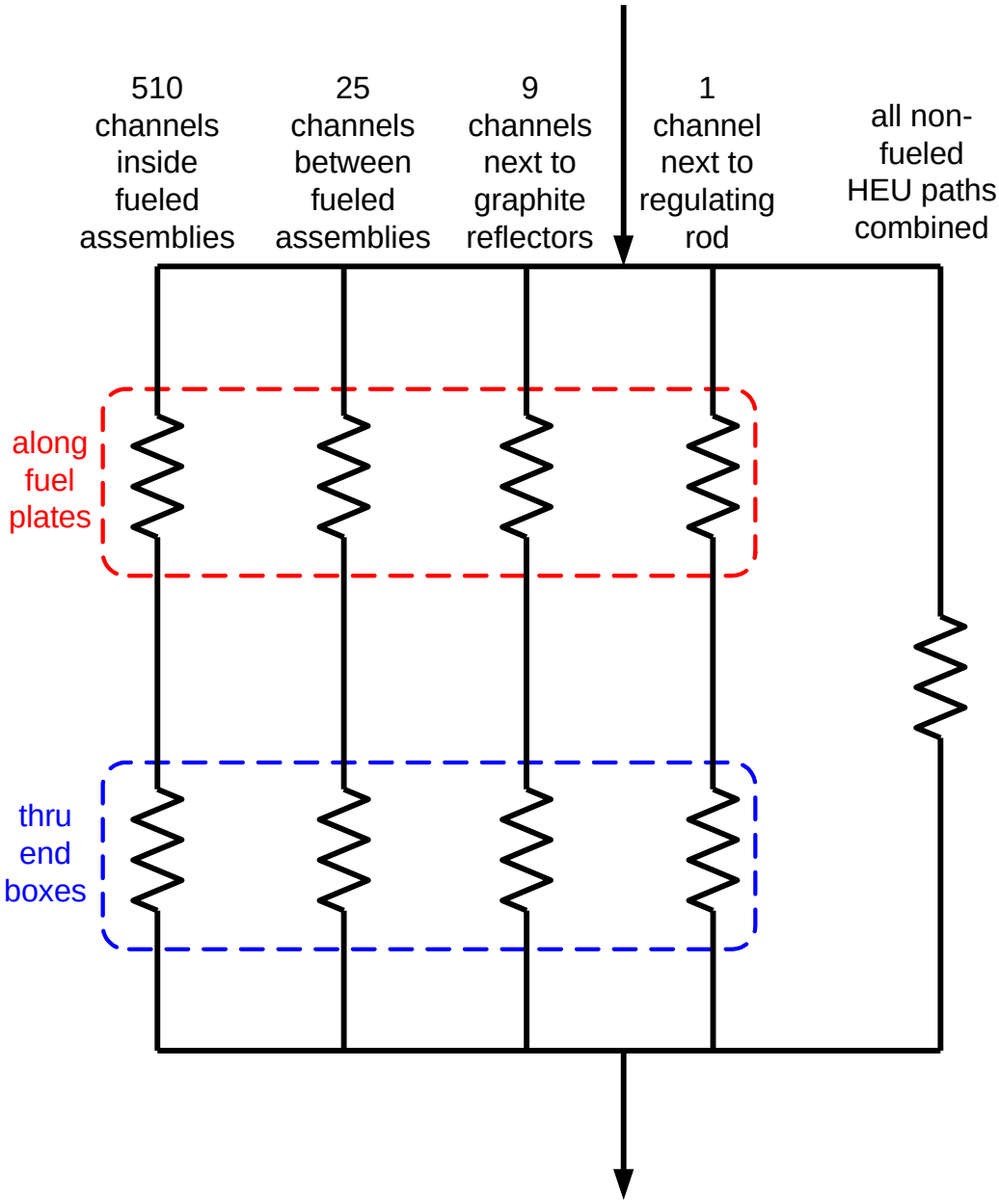


**Figure 4.6-3 – Parallel Flow Paths through the HEU Core**
**(This does not include the gamma shield flow.)**

The hydraulic network for the LEU core in Figure 4.6-4 is similar to the HEU one in Figure 4.6-3, but with added non-fueled bypass types of paths to account for the flow between the beryllium reflectors and the flow through the 0.25-inch holes in these 16 reflectors. (As explained above, the central beryllium reflector is modeled as if it were the same as the other 15.) Also, for the LEU network, in the third parallel hydraulic path, fueled channels next to the graphite reflectors are replaced with fueled channels next to the beryllium reflectors. The LEU hydraulic network also includes the flow through the gamma shield since this is part of the total measured flow.

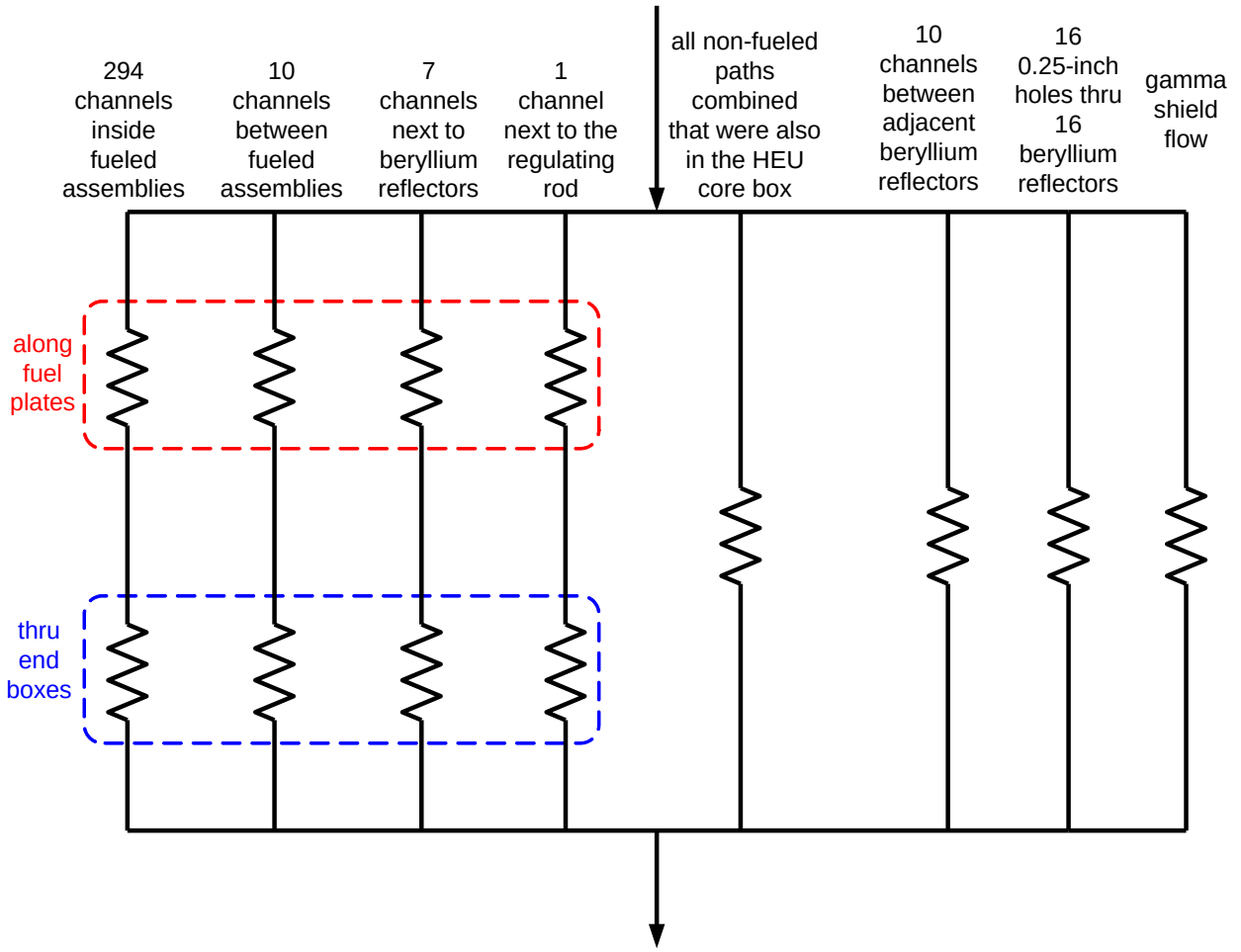


**Figure 4.6-4 – Parallel Flow Paths through the LEU Core Plus the Gamma Shield Flow (This includes all of the flow that passes through the flow meter.)**

The unheated flow that passed between the beryllium reflectors encounters a hydraulic resistance between the reflectors and a second one when it passes through the end boxes to reach the outlet plenum. The second part of this hydraulic resistance will be ignored. This results in slightly more flow being predicted to pass between the beryllium reflectors, leaving less of the total flow to go through the fuel channels. This is on the safer side and makes the analysis simpler. The resistance for the flow through the 0.25-inch diameter holes in the beryllium reflector will be treated as a long straight path with an inlet and an outlet form loss.

In each of the two network diagrams, for each parallel flow path between the source and the sink an equation relating the common pressure difference to the flow rate through the path can be written. This equation for the first HEU path, for example, will provide the flow through only 1 of the 510 identical channels inside fueled assemblies. This flow rate must be multiplied by 510 to obtain the combined flow rate for all 510 identical channels. Since the HEU diagram has 5 parallel paths, it has 5 unknown flow rates and 5 pressure drop versus flow rate equations. The common pressure difference is the $6^{th}$ unknown. The continuity equation provides that the sum of the flow rates represented by the 5 parallel paths in the diagram must equal the total flow rate through the flow network, which is known. Thus, there are 6 equations and 6 unknowns, which can be represented and solved with the aid of a computer spreadsheet.

For turbulent flow, the Moody friction factor is approximated by the Blasius equation:

$$f = 0.316\, Re^{-0.25} \tag{3}$$

where Re is the Reynolds number.

At a sudden contraction or expansion along the flow path, there is only one form loss at the interface and the head loss, i.e., $\rho V^2/2$, is based on the part of the flow path with the smaller flow area. For a sudden expansion from flow area $A_1$ to flow area $A_2$, the K-loss value, $K_{exp}$, is given by:

$$K_{exp} = \left(1 - \frac{A_1}{A_2}\right)^2 \tag{4}$$

Based on Reference 2, for a sudden contraction from flow area $A_1$ to flow area $A_2$, where the inlet to the smaller area is sharp, i.e., square-edged rather than rounded, the K-loss value, $K_{contract}$, for $Re > 10^4$ can be approximated by:

$$K_{contract} = 0.5\left(1 - \frac{A_2}{A_1}\right)^{0.75} \tag{5}$$

For a well rounded entrance the K-loss values can drop to between 0.01 and 0.05. Often when L/D is small $f \times L/D$ is small relative to the form losses and therefore can be ignored.

In the analysis equation 5 is applied to obtain the K-loss value at the entrances to each fueled channel and equation 4 is applied at the exits. In each of the cases the ratio of the smaller area to the larger area is taken to be the total flow area within the unit cell for the fueled assembly divided by the area of the unit cell. This ratio is 5.140/9.364 for the LEU core and 5.190/9.364 for the HEU core. A similar approach is used to determine the K-loss values at the inlet and exit to the end boxes for the fueled channel. Equations 5 and 4 are used again, except that the ratio of the smaller area to the larger area is 4.89/9.364. The form loss values, or K-values, for the end boxes could be added to those for the fueled channels in equation 2 if the flow velocity were the same for both regions. However, the average velocity for the end boxes is a factor of 5.14/4.89

for the LEU fuel and 5.19/4.89 for the HEU fuel. Therefore, equation 2 was used with the K-losses for the end boxes increased by $(5.14/4.89)^2$ for the LEU core and $(5.19/4.89)^2$ for the HEU core. All of theses K-loss values were between 0.2 and 0.3. These are to be compared with typical f L/D values of 4. Thus, the uncertainties in the K-loss values have only a minor effect of the predicted flows.

Each assembly has a symmetrical design with the end box and the top fixture of identical design that enables either end to be inserted into the grid plate. However, the flow area at the bottom is much less than that at the top because the bottom passes through the grid plate. Because the annular square end box cross section has an nominal outer dimension of 2.602 inches and an inner of 2.224 inches, the cross section of the aluminum metal of the end fixture blocks only about 20% of the 3.06-inch square unit cell area. If the area ratios in equations (4) and (5) are taken to be 0.8, then $K_{expansion}$ is 0.04 and $K_{contract}$ is 0.15. The flow area in this region is also about 45% larger than it is in the fueled region and the coolant velocity is proportionately smaller. Thus, these K-losses should be divided by about $1.45^2$ before they are compared with the other hydraulic resistances along the flow path. $0.04/1.45^2 = 0.02$ and $0.15/1.45^2 = 0.07$. Thus, in the analysis the hydraulic resistances of the top end fixtures were ignored.

For the flow in the channel between two adjacent beryllium reflectors, the form losses associated with the flow into and out of the end boxes were set to zero. This produces slightly more predicted flow through these channels and leaves slightly less of the total flow for the fueled channels, which is on the safe side for the analysis. The 0.25-inch holes in the beryllium reflectors were modeled as round ducts that are 29.5 inches long. Base on equations 5 and 4, the inlet and outlet K-loss values for these small holes are 0.5 and 1.0, respectively. Since the outlet of each hole is directly into an end box, there are no additional form losses for these paths.

The hydraulic resistance for the gamma shield path included the hydraulic resistance for the piping that connects the gamma shield to the 10-inch cooling box pipes and the hydraulic resistance through the gamma shield itself. For safety analysis, a minimum bound for this resistance is sufficient because a minimum bound maximizes the gamma shield flow and, in turn, minimizes the remaining portion of the total flow that cools the fuel. Pages 1-25/1-26 of the 1962 operation and maintenance manual[3] show that 3-inch pipes were used. A standard 3-inch pipe has an outer diameter of 3.5 inches and a wall thickness of 0.216 inches. Thus, the inner diameter is $3.5 - 2\times0.216$ inches = 3.068 inches. Photographs of this piping taken during plant maintenance indicate the piping diameter is no greater than 3.5 inches. The gamma shield is about 12 feet below the 10-inch pipes to which it connects. Thus, the piping length is at least 24 feet. For the analysis 24 feet of piping with an inner diameter of 3.068 inches was assumed. In order for the flow path there must be the equivalent of at least two 90° turns for the flow to go down to the gamma shield and return back up. A 90° elbow has a form-, or K-loss of 0.9. There are additional hydraulic losses where the flow enters and where the flow exits the gamma shield. Thus, a low estimate of the total K-loss for the gamma-shield path is 2.0. This value is used in the analysis of the gamma-shield flow.

### 4.6.5 Hydraulic Results

The RINSC reactor technical specifications indicates the maximum outlet temperature is 125° F, the maximum power is 2.4 MW, the minimum flow rate is 1580 gpm, and the minimum water depth is 23.54 feet above the active core. For a water temperature of 115° F the corresponding water density is 989.8 kg/$m^3$. The added pressure due to the weight of the water at 23.54 feet is 989.8 kg/$m^3$ × 9.80665 m/$s^2$ × 23.54 ft × 0.0254 × 12 m/ft = 69645 Pa = 0.696 bar. Narragansett, Rhode Island is at 20 feet above sea level, where atmospheric pressure is 1.013 bar. Thus, the absolute pressure at the top of the active core is 1.013 + 0.696 bar = 1.709 bar. Since the limiting safety setting for the water depth is 23.8 ft (23 ft 9.6 in.), which is 3.1 inches higher than the 23.54 ft (23 ft 6.5 in) safety limit, the added pressure due to the weight of the water is 0.704 bar and the pressure at the top of the active core is 1.717 bar. In the analysis 1.7 bar was used.

Since in each of the two primary flow loops the flow meter is located after the heat exchanger and before the reactor inlet, the water density should be based on the inlet temperature when relating gpm to kg/s. Based on the above technical specification limiting power (2.4 MW), flow rate (1580 gpm), and outlet temperature (125° F), the core inlet temperature is 114.5° F. This value is rounded up to 115° F and is used for the flows through and between the beryllium reflectors. For the heated channels 120° F was used so that density and the viscosity of the heat paths in the analysis would be close to expected average values over the core length. For a pressure of 1.7 bar, the 1996 NIST/ASME Steam Tables show that for 115 and 120° F, the water density is 989.8 and 988.6 kg/$m^3$, respectively.

Tables 4.6-3 and 4.6-4 show key parameter values from the calibration of the HEU hydraulics model at 1500 gpm. This analysis provides the value for $C_1$ in equation 1 of 33.728 for pressure drop, $\Delta P$, in pascals, which is needed for the hydraulic analysis of the LEU core. Table 4.6-5 shows key values from the hydraulic analysis of the LEU core at 1580 gpm. The four columns labeled "fueled paths" correspond to the first four parallel paths shown in Figure 4.6-4. The two columns labeled "non-fueled paths" correspond to the sixth and seventh parallel paths shown in Figure 4.6-4. The fifth parallel path in Figure 4.6-4 is represented by equation 1. The flow rate for this path is 18.06 kg/s, 289.2 gpm, based on 115° F water, as is shown in Table 4.6-6. The pressure drop from assembly inlet to the outlet plenum, 6168 Pa, is also shown in this table, along with the fraction of the total metered flow through fueled channels, 0.7073. This is to be compares with the 0.8597 value provided in Table 4.6-4 which was obtained by dividing the total flow past the fuel plates by the total metered flow, including the 76.2 gpm gamma shield flow. This value is less than the 90.33% value in Table 4.6-1, which considers only the 1500 gpm through the core box, but not the additional 76.2 gpm through the gamma shield.

The hydraulics results needed for the thermal analysis are the flow rates of the individual fueled channels. As will be shown later, the highest power fuel plate among the 308 in the core is the one in assembly D6 immediately adjacent to the central beryllium reflector. As Table 4.6-5 shows, among the four types of fueled channels, the one with the lowest flow rate, 0.1893 kg/s, is the one adjacent to a beryllium reflector. However, this channel is heated from only one side. The fueled channel type with the next lowest flow rate is the one formed between two fuel plates of the same assembly. This type of channel is heated from two sides and has a flow rate, as show

in Table 4.6-5, of 0.2210 kg/s. Although this flow rate is only 17% greater than the lowest flow rate, the power input to the channel is about double. Thus, the limiting channel is the one formed between the two fuel plates of assembly D6 that are closest to the central beryllium reflector. Therefore, this single channel with this flow rate will be studied to determine at what powers nucleate boiling, flow instability, and critical heat flux are each predicted to occur.

**Table 4.6-3 – HEU Hydraulics Model Calibration at 1500 gpm**
**(The gamma shield flow is not part of the calibration and is not part of the 1500 gpm.)**

| | Fueled Paths | | | | |
|---|---|---|---|---|---|
| item | between internal plates | between end plates | next to beryllium reflectors | next to regulating rod | gamma shield |
| number of channels | 510 | 25 | 9 | 1 | 1 |
| channel width, in. | 2.62 | 2.62 | 2.62 | 2.62 | |
| channel thickness, in. | 0.107 | 0.161 | 0.087 | 0.128 | |
| path length, inches | 25 | 25 | 25 | 25 | 288 |
| wetted perimeter correction, in | 0 | -0.030 | 0.016 | -0.110 | 0 |
| area correction, in^2 | 0 | 0 | 0.03953 | 0 | 0 |
| flow area, in^2 | 0.2803 | 0.4218 | 0.2675 | 0.3354 | 7.3927 |
| flow area, m^2 | 1.809E-04 | 2.721E-04 | 1.726E-04 | 2.164E-04 | 4.769E-03 |
| wetted perimeter, in. | 5.454 | 5.532 | 5.430 | 5.386 | 9.638 |
| wetted perimeter, m | 0.1385 | 0.1405 | 0.1379 | 0.1368 | 0.2448 |
| hydraulic diameter, m | 5.222E-03 | 7.747E-03 | 5.005E-03 | 6.326E-03 | 7.793E-02 |
| hydraulic diameter, in. | 0.2056 | 0.3050 | 0.1970 | 0.2491 | 3.068 |
| temperature, F | 120 | 120 | 120 | 120 | 120 |
| density, kg/m^3 | 988.6 | 988.6 | 988.6 | 988.6 | 988.6 |
| viscosity, Pa-s | 5.569E-04 | 5.569E-04 | 5.569E-04 | 5.569E-04 | 5.569E-04 |
| 1 velocity head, Pa | 345.8 | 519.0 | 329.8 | 424.5 | 503.5 |
| Reynolds number | 7,754 | 14,091 | 7,257 | 10,407 | 139,623 |
| friction factor, Blasius | 0.0337 | 0.0290 | 0.0342 | 0.0313 | 0.0163 |
| friction factor × length/diameter | 4.095 | 2.377 | 4.344 | 3.140 | 1.535 |
| K-loss upper inlet | 0.273 | 0.273 | 0.273 | 0.273 | |
| K-loss upper outlet | 0.199 | 0.199 | 0.199 | 0.199 | |
| K-loss lower inlet | 0.287 | 0.287 | 0.287 | 0.287 | |
| K-loss lower outlet | 0.228 | 0.228 | 0.228 | 0.228 | |
| K-loss total | 1.052 | 1.052 | 1.052 | 1.052 | 2 |
| flow rate / channel, kg/s | 0.1496 | 0.2757 | 0.1394 | 0.1982 | 4.7590 |
| flow rate / channel (115° F), gpm | 2.395 | 4.414 | 2.232 | 3.174 | 76.208 |
| channel velocity (120° F), m/s | 0.836 | 1.025 | 0.817 | 0.927 | 1.009 |

### 4.6.6 The PLTEMP/ANL V4.0 Code

**Table 4.6-4 – Additional Values for HEU Hydraulics Model Calibration at 1500 gpm**

| Item | Value |
|---|---|
| **Combine core box bypass channel common to HEU & LEU cores** | |
| **Flow coefficient** | **33.728*** |
| **Flow exponent** | **1.8** |
| **Flow rate, gpm @ 115° F** | **145.0** |
| **Flow rate, kg/s** | **9.0548** |
| **Pressure drop – top of core to outlet plenum, Pa** | **1778** |
| **Fraction of total metered flow thru fueled channels**** | **0.8597** |

***For pressure drop in pacals**
****The total includes gamma shield flow.**

The thermal analysis is performed with the aid of the PLTEMP/ANL V4.0 Code.[4] This code can model an entire core, a number of fuel assemblies, or a series of fuel plates and coolant channels that form a portion of an assembly. This code is capable of analyzing a large series of parallel fuel plates separated by intervening coolant channels, such as occurs in the RINSC reactor. The code is sufficiently sophisticated to thermally couple all of the coolant channels of a single assembly rather than simply assume that half of the power of each plate comes out of either face. The code has a hydraulics model that can determine the flow distribution among core assemblies and within individual channels or the user can specify the flow rate for each coolant channel, as will be done for the RINSC reactor.

PLTEMP was first created in 1984, and has evolved over many versions to the present day. It is a FORTRAN program that obtains a steady-state flow and temperature solution for a nuclear reactor core, or for a single fuel assembly. It is based on an evolutionary sequence of "PLTEMP" codes in use at ANL for the past 26 years.[5-11] Fueled and non-fueled regions are modeled. Each fuel assembly consists of one or more plates or tubes separated by coolant channels. The temperature solution is effectively two-dimensional. It begins with a one-dimensional solution across the fuel plates/tubes within a given fuel assembly, at the entrance to the assembly. The temperature solution is repeated for each axial node along the length of the coolant channel. The geometry may be either slab or radial, corresponding to fuel assemblies made from a series of flat (or slightly curved) plates, or from nested tubes.

A variety of thermal-hydraulic correlations are available with which to determine safety margins such as Onset-of- Nucleate boiling (ONB), critical heat flux (CHF), and onset of flow instability. Coolant properties for either light or heavy water are obtained from FORTRAN functions rather than from tables. The code is intended for thermal-hydraulic analysis of research reactor performance in the sub-cooled boiling regime. Both turbulent and laminar flow regimes can be modeled. Options to calculate both forced flow and natural circulation are available. A general search capability is available (see Appendix XI of Reference 4) to greatly reduce the reactor analyst's time. The RINSC reactor operates with light water coolant in the sub-cooled boiling regime, under laminar or turbulent flow conditions created by natural circulation or forced flow. It is clear that the PLTEMP code is capable of modeling steady-state operating conditions for RINSC.

Validation of PLTEMP/ANL has followed standard practice in any code development task, where comparisons are made with other codes, with measurements, and with hand calculations

where possible. Many examples of validation are given in the PLTEMP/ANL V4.0 manual, and in References 5-11.

**Table 4.6-5 – LEU Hydraulics Analysis Values (1580 gpm)**

| | Fueled Paths | | | | Non-Fueled Paths | |
|---|---|---|---|---|---|---|
| item | between internal plates | between end plates | next to beryllium reflectors | next to regulating rod | between beryllium reflectors | 0.25" hole in beryllium reflector |
| number of channels | 294 | 10 | 7 | 1 | 10 | 16 |
| channel width, in. | 2.62 | 2.62 | 2.62 | 2.62 | 2.62 | |
| channel thickness, in. | 0.088 | 0.112 | 0.0645 | 0.1035 | 0.017 | |
| path length, inches | 25 | 25 | 25 | 25 | 25 | 29.5 |
| wet. perim. correct., in | 0 | -0.030 | 0.012 | -0.110 | 0.054 | 0 |
| area correction, in^2 | 0 | 0 | 0.03945 | 0 | 0.07889 | 0 |
| flow area, in^2 | 0.2306 | 0.2934 | 0.2084 | 0.2712 | 0.1234 | 0.0491 |
| flow area, m^2 | 1.487E-04 | 1.893E-04 | 1.345E-04 | 1.749E-04 | 7.963E-05 | 3.167E-05 |
| wetted perimeter, in. | 5.416 | 5.434 | 5.381 | 5.337 | 5.328 | 0.7854 |
| wetted perimeter, m | 0.1376 | 0.1380 | 0.1367 | 0.1356 | 0.1353 | 0.01995 |
| hydraulic diameter, m | 4.325E-03 | 5.486E-03 | 3.936E-03 | 5.162E-03 | 2.354E-03 | 6.350E-03 |
| hydraulic diameter, in. | 0.1703 | 0.2160 | 0.1549 | 0.2032 | 0.09267 | 0.25 |
| temperature, F | 120 | 120 | 120 | 120 | 115 | 115 |
| density, kg/m^3 | 988.6 | 988.6 | 988.6 | 988.6 | 989.8 | 989.8 |
| viscosity, Pa-s | 5.569E-04 | 5.569E-04 | 5.569E-04 | 5.569E-04 | 5.842E-04 | 5.842E-04 |
| 1 velocity head, Pa | 1116.5 | 1445.3 | 1002.4 | 1355.5 | 558.4 | 1300.0 |
| Reynolds number | 11539 | 16654 | 9949 | 15175 | 4236 | 17437 |
| friction factor, Blasius | 0.0305 | 0.0278 | 0.0316 | 0.0285 | 0.0392 | 0.0275 |
| frict. factor × Leng/Dia. | 4.476 | 3.219 | 5.105 | 3.502 | 10.57 | 3.245 |
| K-loss upper inlet | 0.275 | 0.275 | 0.275 | 0.275 | 0.275 | 0.5 |
| K-loss upper outlet | 0.203 | 0.203 | 0.203 | 0.203 | 0.203 | 1.0 |
| K-loss lower inlet | 0.287 | 0.287 | 0.287 | 0.287 | | |
| K-loss lower outlet | 0.228 | 0.228 | 0.228 | 0.228 | | |
| K-loss total | 1.048 | 1.048 | 1.048 | 1.048 | 0.4787 | 1.5 |
| flow rate / channel, kg/s | 0.2210 | 0.3200 | 0.1893 | 0.2864 | 0.08373 | 0.05080 |
| flow rate / channel, gpm* | 3.539 | 5.125 | 3.032 | 4.586 | 1.341 | 0.814 |
| channel velocity, m/s** | 1.503 | 1.710 | 1.424 | 1.656 | 1.062 | 1.621 |

***density evaluated at 115° F**
****density evaluated at 120° F**

### 4.6.7 Hot Channel Factors

Table 4.6-7 lists the hot channel factors for the LEU core. This table lists random and systematic sources of uncertainty separately. The random sources can affect any fuel plate or coolant channel. However, it is unlikely that all of the random sources can adversely affect the limiting location(s) in the reactor core simultaneously. The first four random sources relate to the distribution of power. The final two random sources relate to channel spacing and flow distribution.

The three systematic sources affect all regions of the core essentially equally and are directly included in the thermal calculation by increasing the reactor power, decreasing the reactor flow, and decreasing the Nusselt number, which provides the film coefficient. Thus, the systematic errors are directly incorporated into the physics of the problem. The combined random errors produce four hot channel factors, shown in red in the table, that are multiplicative factors applied to calculated temperature rises, heat fluxes, and flow rates. The random errors produce multipliers and divisors that are used to adjust calculated quantities obtained from the physics of the problem.

**Table 4.6-6 – Additional Values for the LEU Core at 1580 gpm**

| Item | Value |
|---|---|
| **Combine core box bypass channel common to HEU & LEU cores** | |
| **Flow coefficient** | **33.728*** |
| **Flow exponent** | **1.8** |
| **Flow rate, gpm @ 115° F** | **289.2** |
| **Flow rate, kg/s** | **18.06** |
| **Gamma shield flow** | |
| **Flow rate, gpm @ 115° F** | **146.7** |
| **Flow rate, kg/s** | **9.1653** |
| **Pressure drop – top of core to outlet plenum, Pa** | **6168** |
| **Fraction of total metered flow thru fueled channels**** | **0.7073** |

***For pressure drop in pacals**
****The total includes gamma shield flow.**

After a PLTEMP/ANL solution is obtained that includes the systematic factors, the random combined hot channel factors for channels $F_{bulk}$ and $F_{film}$ are used to adjust the clad surface temperatures via the following relationship.

$$T_{surf} = T_{in} + F_{bulk}\,\Delta T_b + F_{film}\,\Delta T_h) \qquad (6)$$

where $T_{surf}$ is the local clad surface temperature, $T_{in}$ is the reactor inlet coolant temperature, $\Delta T_b$ is the coolant inlet temperature rise from the inlet to the local elevation, $\Delta T_h$ is the local film temperature rise from the bulk coolant to the clad surface, $F_{bulk}$ is the hot channel factor for bulk coolant temperature rise from reactor inlet to the local elevation of concern, $F_{film}$ is the hot channel factor for the local film temperature rise at the location of concern on the fuel plate surface.

$F_q$ and $F_w$ may be needed to incorporate the effects of uncertainties in heat flux and flow in the limiting criterion. For example, departure from nucleate boiling is a function of local heat flux.

The first two random uncertainties, which are caused by variations in the fuel meat thickness and $^{235}U$ homogeneity, are labeled "local" in that they are assumed to be hot-spot effects that affect the heat flux in only a local area with only minor perturbations in bulk coolant temperature. Since these sources of uncertainty affect the distribution of fuel rather than the total amount of it, the bulk coolant outlet temperature is not affected by these sources.

In most instances the third and fourth random uncertainties affect only one of two plates that bound a coolant channel. Therefore, the effect on bulk coolant temperature rise, as represented by the corresponding $F_{bulk}$ component, is half as great. For example, a 3% fuel overloading in a single plate would produce a 1.030 $F_q$ subcomponent, but only a 1.015 $F_{bulk}$ subcomponent.

**Table 4.6-7 – Hot Channel Factors**

| uncertainty | effect on bulk ΔT, fraction | value, inches or mm | toler-ance, inches or mm | toler-ance, fraction | hot channel factors: heat flux, $F_q$ | hot channel factors: channel flow rate, $F_w$ | hot channel factors: channel temper-ature rise, $F_{bulk}$ | hot channel factors: film temper-ature rise, $F_{film}$ |
|---|---|---|---|---|---|---|---|---|
| ***random errors*** | - | | | | | | | |
| fuel meat thickness (local) | | | | 0.00 | 1.00 | | | 1.00 |
| U235 homogeneity (local) | | | | 0.20 | 1.20 | | | 1.20 |
| U235 loading per plate | 0.50 | | | 0.03 | 1.03 | | 1.015 | 1.03 |
| power density | 0.50 | | | 0.10 | 1.10 | | 1.050 | 1.10 |
| channel spacing | 1.00 | 0.088 | 0.006 | 1.073 | | 1.129 | 1.129 | 1.027 |
| flow distribution | 1.00 | | | 0.20 | | 1.20 | 1.20 | 1.157 |
| random errors combined | | | | | 1.23 | 1.24 | 1.24 | 1.28 |
| ***systematic errors*** | | | | | | | | |
| power measurement | 1.00 | | | 0.00 | 1.00 | | 1.00 | 1.00 |
| flow measurement | 1.00 | | | 0.00 | | 1.00 | 1.00 | 1.00 |
| heat transfer coefficient | | | | 0.20 | | | | 1.20 |
| systematic errors combined | | | | | 1.00 | 1.00 | 1.00 | 1.20 |
| product of random & systematic combinations | | | | | 1.23 | 1.24 | 1.24 | 1.53 |

The yellow colored boxes in Table 4.6-7 identify key independent variables. A line-by-line description of this table follows:

fuel meat thickness (local)
This is a result of the manufacturing process. When the fuel plates are rolled to the desired size, the fuel meat thickness in some regions of the plate may be thicker by as much as a specified tolerance. Other regions of the fuel meat can be too thin and result in less than the nominal heat flux. The amount of $^{235}U$ in each plate is assumed to be measured separately so that the fuel meat thickness only affects the distribution of power within the plate. For the LEU fuel, which is dispersion fuel, the manufacturing specification requires that measurements of fuel density are made through the thickness of the fuel over the width and length of one face of the clad. These measurements simultaneously measure the effects of fuel loading differences regardless of whether they are result of variations in fuel meat thickness or local lack of fuel homogeneity. The fluctuation in the uranium homogeneity or density, based on TRTR-6 specification 3.4.2,[12] the variation in average fuel section is ±20%. Thus, for the LEU fuel a value of 0.00 is used for the fuel meat thickness tolerance and a value of 0.20 is used for the $^{235}U$ homogeneity tolerance. (The LEU fuel plate variation specification, as shown by EG&G drawing number 422264, is 0.050±0.002, which is 4%. If this were included in Table 4.6-7, the three entries under "fuel meat thickness (local)" would be 0.04, 1.04, and 1.04, respectively. Nothing else in the table would change because the effect is in the third decimal place.)

$^{235}U$ homogeneity (local)
This is a tolerance on how well the $^{235}U$ is mixed with the other ingredients that are in the fuel meat. The amount of $^{235}U$ in each plate is assumed to be measured separately so that the $^{235}U$ homogeneity only affects the distribution of power within the plate. The 0.20 tolerance in Table 4.6-7 is explained in the previous paragraph.

$^{235}U$ loading per plate
This is a tolerance on the weight of $^{235}U$ that is to go into a plate. The allowed variation in fuel plate loading is 2.8% and causes the same amount of variation in heat generation in the plate. Therefore, 0.03 is used.

power density
This uncertainty is assumed to be a result of the physics calculations and can result in more power being in a particular plate than was predicted and used in the nominal thermal-hydraulic analysis. The 10% value for both fuel types is a result of engineering judgment.

channel spacing, inches
This tolerance is obtained by dividing the nominal channel thickness by the minimum channel thickness allowed by the dimensional tolerances on the drawings. The LEU fuel assembly drawing shows that the each of the 21 channels must have a channel thickness that is between 0.082 and 0.094 inches. This is taken to correspond to 0.088±0.006 inches.

For plate geometry where the hydraulic diameter can be approximated as twice the channel thickness, the formulas for obtaining the $F_{bulk}$ and $F_{film}$ subcomponents due to channel spacing tolerances can be found on page 5 in Reference 13. They are as follows:

$$F_{bulk} = \left( \frac{t_{nc}}{t_{hc}} \right)^{\frac{3}{2-\alpha}} \quad (7)$$

$$F_{film} = \left( \frac{t_{nc}}{t_{hc}} \right)^{\frac{0.4+\alpha}{2-\alpha}} \quad (8)$$

where $t_{nc}$ and $t_{hc}$ are the nominal channel thickness and the minimum (or hot) channel thickness, respectively. $\alpha$ is the value of the Reynolds number exponent in the friction factor relationship. In this relationship, friction factor, f, is approximated as being proportional to $Re^{-\alpha}$. For turbulent flow $\alpha$ is typically 0.2 or 0.25. 0.25 was used in Table 4.6-7. In this table, 1.073 was obtained by dividing 0.088 inches by (0.088 – 0.006) inches.

flow distribution

This uncertainty is the result of the hydraulic analysis that is used to determine the distribution of flow through the reactor. This is a local effect that does not systematically affect all coolant channels. Quantities such as friction factors and form losses and the influence of grid plates can not be precisely predicted. Although hydraulic models often predict that channels of equal thickness have the same channel average velocity, seemingly slight variations can cause significant differences. A value of 0.20 was assumed to account for variations in flow distribution.

random errors combined

As suggested in the Reference 13 treatment of hot channel factors, it is unlikely that all of the random errors and uncertainties will occur together at the most limiting location in the reactor and that each will adversely affect reactor performance. Therefore, the random subcomponents, $F^i$, of each hot channel factor, F, are combined statistically, i.e., $F = 1 + \sqrt{\sum_i \left(F^i - 1\right)^2}$ .

power measurement

This is a tolerance of the meter that is used to measure power and, if present, would affect all fuel plates essentially equally. The power level used in the analytical calculations is the true power. The power measurement uncertainty is included in the interpretation of the results where a measured power of 2.0 MW with a measurement uncertainty of 0.4 MW, for example, would be treated in the interpretation of the results of corresponding to a true power of 2.4 MW. A value of 0.00 is shown in green in Table 4.6-7 because this is the value used in the analytical modeling.

flow measurement

Analogous to the tolerance on power measurement, this is a tolerance of the meter that is used to measure power and, if present, would affect all fuel plates essentially equally. The flow rate used in the analytical calculations is the true flow rate. The flow measurement uncertainty is included in the interpretation of the results and causes a measured flow rate to be interpreted as a

true flow rate of a significantly lesser value. A value of 0.00 is shown in green in Table 4.6-7 because this is the value used in the analytical modeling.

heat transfer coefficient

This is due to uncertainties in the correlations for Nusselt number that are used to determine values of heat transfer coefficient. If the Nusselt number correlations that are used in the analysis predict values that are too large, then the predicted temperatures on all clad surfaces will be lower than would otherwise be experienced by the reactor. This is a core-wide effect rather than one that is random in location. A value of 0.20 is judged to be a reasonable value for this uncertainty and is show in green in the table.

systematic errors combined

Because systematic errors, such as an error in reactor power and flow measurement, affect all locations within the reactor at the same time, it is reasonable to expect that all of them could be present at the limiting location(s). Therefore, the systematic subcomponents are combined multiplicatively, i.e., $F = \prod_i F^i$. Because in the PLTEMP/ANL analysis the systematic errors are included in the physics of the problem, this product is not directly used in the analysis.

product of random and systematic parts

Each of these products provides a hot channel factor, which represents the combination of all of its random and systematic subcomponents. This combination of subcomponents is not directly used in the analysis. As explained above, the value shown in Table 4.6-7 do not include the power and flow measurement uncertainties.

### 4.6.8 Thermal Analysis

EG&G Drawing 422873 indicates that for the LEU fuel plate, the width of the fuel meat is between 2.32 and 2.47 inches and the length of the fuel meat is between 22.50 and 24.00 inches. Average values of 2.395 and 23.25 inches, respectively, were used in the neutronic analysis and is used in the thermal analysis. These dimensions are important because they are used to determine heat transfer area, which, in turn, is used to determine heat flux.

There are 14 fuel assemblies, or elements, in the equilibrium core. Each has 22 fuel plates, for a total of 14 × 22, or 308, in the core. The highest power fuel plate among these 308 is the one immediately adjacent to the beryllium reflector in assembly D6. When the reactor is operating at 2 MW, the power in this plate is 9.653 kW. In the neutronics analysis the fuel meat in each plate in assembly D6 was subdivided into 16 vertical stripes along the width of the plate and 17 axial layers along the length of the plate. The meat thickness was not subdivided. The largest value of volumetric heat generation rate among these 16 × 17, or 272, subvolumes was 704 W/cc. The highest volumetric heat generation rate in the entire core was 712 W/cc, which is only 1.1% larger, occurs in the closest plate to the center of the core in assembly E6

The axial power shapes of all 16 stripes of the highest power fuel plate in the core (plate 1 of D6) are almost coincident, as is shown in Figure 4.6-5. The heavy blue dashed line in the figure shows the axial power shape of all 16 stripes taken together, which is used in the thermal analysis. Figure 4.6-6 shows that the highest power stripe of this plate is only 0.6% greater than

that of the average. The power is of the first three plates of Assembly D6 for 2.0 MW operation are shown in the rose colored rectangles of Table 4.6-8. The flow rates for the adjacent channels for a total core flow rate of 1580 gpm of 115° F water are shown in the turquoise rectangles in this figure. While channel 1 in the figure has only 86% of the flow as in either of the other two, it is heated from only one side. The most limiting channel is obviously channel 2, which is heated by the first two plates.

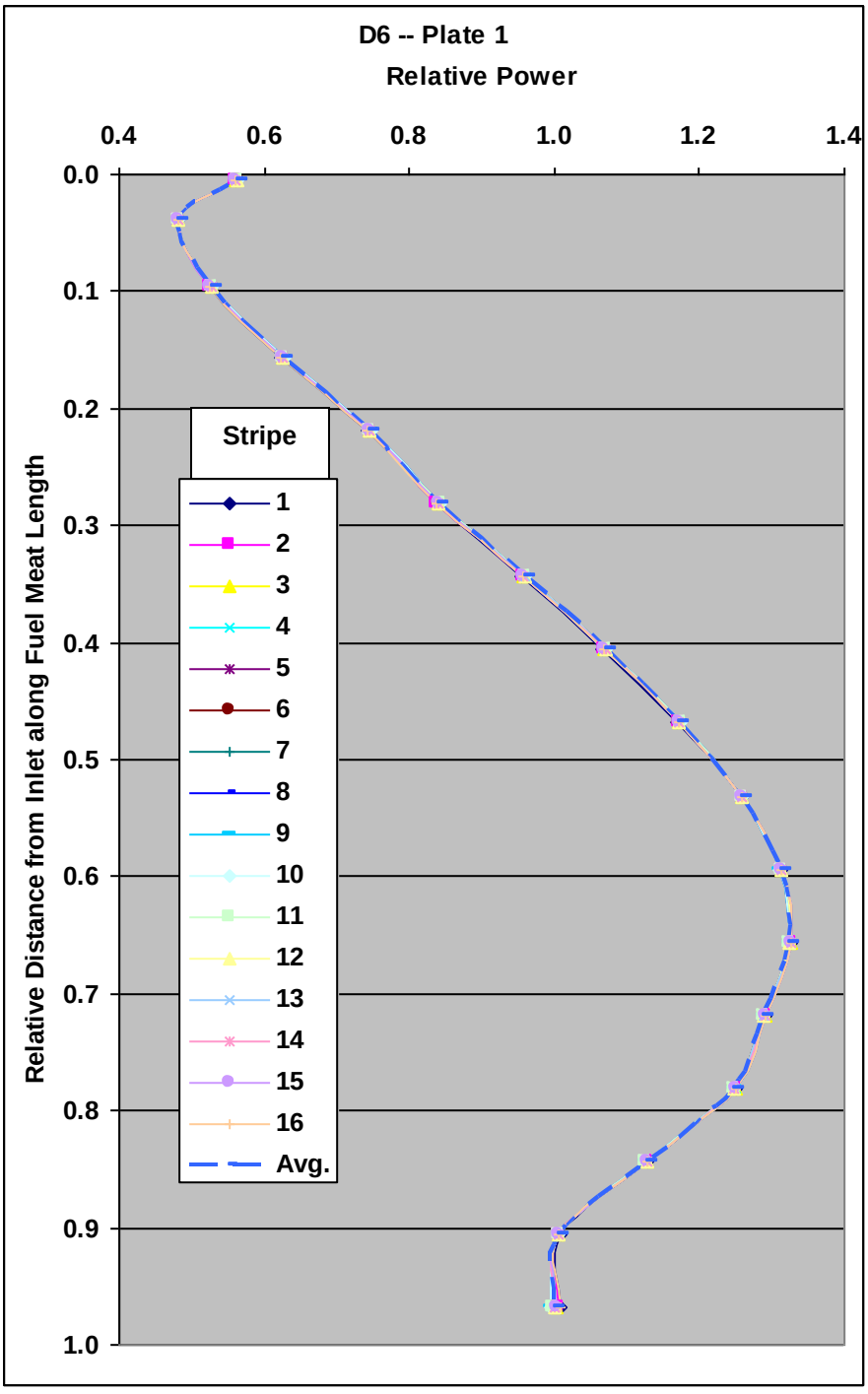


**Figure 4.6-5 – Axial Power Shapes for Assembly D6**

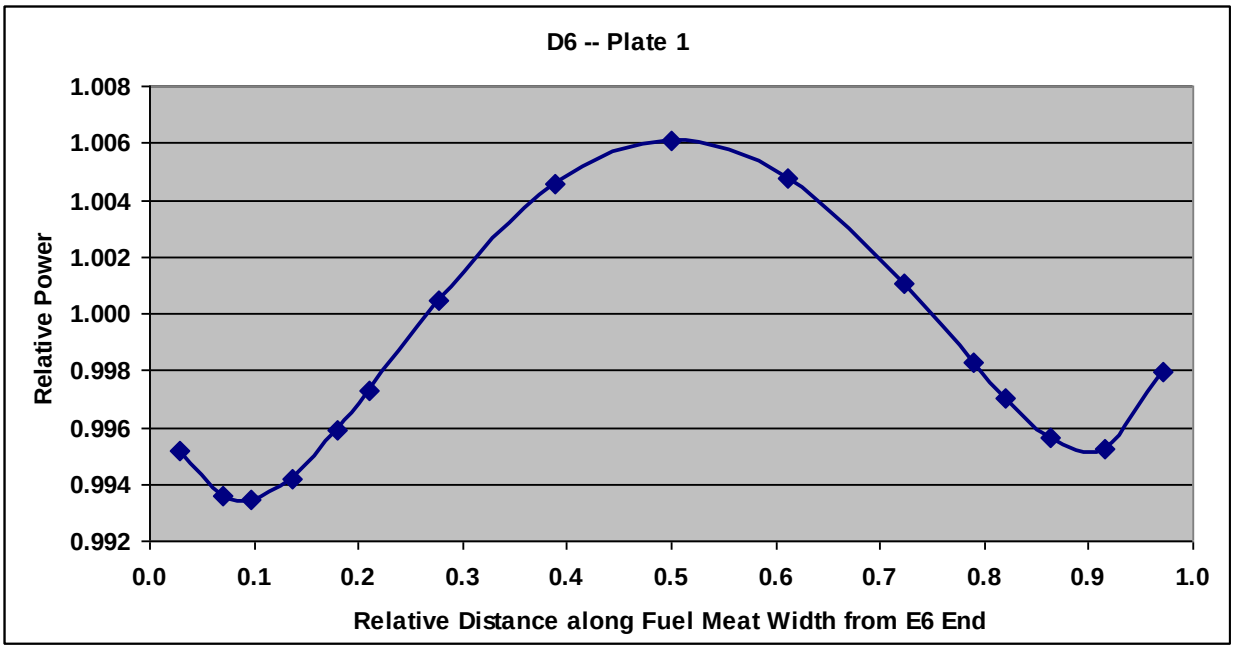


**Figure 4.6-6 – Power Shape along the Width of Plate 1 of Assembly D6**

For the analysis, channel 2 will be analyzed and assumed to be bounded on both sides by plate 1, which is the plate with the highest power. This was done to keep the analysis simple and easy to explain and verify. Since the average power of the first two plates is 96.8 % of the power of first plate, a more detail analysis would predict a slightly larger thermal margin than is being predicted by the single-channel model. Because of assumed symmetries, only a half of plate 1 and the flow of only half of channel 2 need be analyzed. The structure of PLTEMP/ANL, however, requires that each plate be bounded by two channels. Therefore, plate 1 bounded by two channels, each with half of the channel thickness and flow of channel 2, was analyzed.

| 0 kW (Reflector) | 0.1893 kg/s | 9.653 kW | 0.2210 kg/s | 9.039 kW | 0.2210 kg/s | 8.609 kW |
|---|---|---|---|---|---|---|
| Plate | - | 1 | - | 2 | - | 3 |
| Channel | 1 | - | 2 | - | 3 | - |

**Table 4.6-8 – Flow Rates and Powers of the First Three Fuel Plates and Channels of Assembly D6 for Reactor Operation at 2.0 MW and 1580 gpm**

The pressure over the length of the core and the core inlet temperatures are taken to be 1.7 bar and 115° F, respectively. These were chosen to correspond to the Technical Specification limiting values, as explained above in section 4.6.6. The 1.7 bar corresponds to the pressure at the top of the active core. As Table 4.6-6 shows, the pressure drop due to hydraulic resistance from the top of the active core to the outlet plenum for a flow rate of 1580 gpm is 6168 Pa, or 0.06168 bar. However, this is offset by the pressure increase due to the increase in the water

depth over the 25-inch length of the fuel plate. This pressure increase is 989.8 kg/m$^3$ × 9.80665 m/s$^2$ × 25 inches × 0.0254 m/inch = 6164 Pa = 0.06164 bar.

### 4.6.9 Verification of Onset of Nucleate Boiling and Flow Instability Results of Steady-State Thermal Analysis

Before presenting the results of many PLTEMP/ANL code calculations, it is worthwhile to demonstrate that the code predictions for the powers at which the onset of nucleate boiling and the onset of flow instability occur are as expected. Therefore, hand calculations were made with the aid of computer spreadsheets and compared with code values for the limiting reactor flow rate of 1580 gpm. Table 4.6-9 summarizes the key results from the hand calculation of the onset of nucleate boiling and provides comparisons with a few PLTEMP/ANL predictions. The code has a search capability that enables the code to iteratively adjust the power and calculate new state-state solutions until the lowest power at which the onset of nucleate boiling occurs is found. The code results indicate that the onset of nucleate boiling first occurs when the power of the single fuel plate in the model is at 22.80 kW and that the limiting axial location is the 13$^{th}$ axial layer from the inlet. Onset of nucleate boiling is achieved at the 12$^{th}$, 13$^{th}$, and 14$^{th}$ axial layers essentially simultaneously. It was arbitrarily decided to focus on the 13$^{th}$ layer. In the hand calculation, a single channel heated from two sides by two identical halves of a fuel plate is modeled. This is analytically equivalent to a single fuel plate bounded by two half channels. Figure 4.6-7 provides a listing of the PLTEMP/ANL V4.0 input that was used to produce the PLTEMP/ANL results.

ONB occurs when the surface temperature of the fuel plate is ΔTsat degrees above the local coolant saturation temperature. In the code analysis, ΔTsat is obtained from the Bergles and Rohsenow correlation.[14] The surface temperature is obtained by adding the bulk coolant temperature at the middle of the 13$^{th}$ level to the film temperature rise for the 13$^{th}$ node. The bulk coolant temperature is obtained by summing the bulk coolant temperature rise to the middle of the 13$^{th}$ layer and the coolant inlet temperature. The following specifics about PLTEMP/ANL need to be observed in order to accurately reproduce the PLTEMP/ANL clad surface and temperature at the clad surface that corresponds to the onset nucleate boiling:

1. Bulk coolant temperature rise is calculated at the middle of the layer rather than at the exit. It is first calculated without including any of the random hot channel factors and then multiplied by the random hot channel factor for bulk coolant temperature rise.

2. The film coefficient used to calculate the film temperature rise is based on coolant properties that are evaluated at the bulk coolant temperature at the exit of the layer calculated without any hot channel factors applied. Once the film coefficient is determined in this manner, it is divided by the global hot channel factor on film coefficient. This film coefficient is used to determine the film temperature rise, but as calculated does not including the random hot channel factor for ΔT film. Therefore, this film temperature rise is multiplied by the random hot channel factor for ΔT film to obtain the final values of film temperature rise.

3. In the calculation of ΔTsat with the Bergles and Rohsenow correlation, the heat flux value used in the correlation includes the random hot channel factor on heat flux.

**Table 4.6-9 – Verification of PLTEMP/ANL Onset of Nucleate Boiling Prediction at the Limiting Axial Location for a Core Flow Rate of 1580 gpm**

| Quantity | Hand Calculation | PLTEMP |
|---|---|---|
| Channel Dimensions | | |
| Thickness, in | 0.088 | |
| Width, in | 2.62 | |
| Heated Length, in | 23.25 | |
| Heat Width, in | 2.395 | |
| | | |
| Wetted Perimeter, m | 0.1376 | |
| Hydraulic Diameter, m | 0.004325 | |
| Heat Transfer Area (2 Faces), $m^2$ | 0.07185 | |
| | | |
| Channel Flow Rate, kg/s | 0.2210 | |
| Channel Power, kW | 22.80 | |
| Pressure, bar | 1.7 | |
| Inlet Temperature, C | 46.11 | |
| | | |
| Saturation Temperature, C | 115.15 | |
| Cp @ 55 C, kJ/kg-C | 4.1828 | |
| | | |
| At Onset of Nucleate Boiling Location | | |
| Layer | 13 | 13 |
| Channel Power to Middle of Layer, kW | 15.64 | |
| Channel Power to Exit of Layer, kW | 16.56 | |
| Local Peak-to-Average Power | 1.2894 | |
| Bulk Temperature at Middle of Layer w/o Hot Chan. Fac., C | 63.03 | 63.01 |
| Random Hot Channel Factor on ΔT bulk | 1.24 | |
| Bulk Temperature with Hot Channel Factor, C | 67.09 | 67.06 |
| Bulk Temperature at Exit of Layer w/o Hot Chan. Fac., C | 68.32 | |
| Viscosity, Pa-s | 4.3910E-4 | |
| Reynolds Number | 14634 | |
| Thermal Conductivity, W/m-C | 0.65817 | |
| Cp, kJ/kg-C | 4.1867 | |
| Prandtl Number | 2.793 | |
| Nusselt Number without Hot Channel Factors | 74.55 | |
| Global Film Coefficient Hot Channel Factor | 1.2 | |
| Film Coefficient with Hot Channel Factor, $W/m^2$-C | 9454 | |
| Heat Flux without Hot Channel Factors, $MW/m^2$ | 0.4092 | 0.4091 |
| Random Hot Channel Factor on ΔT film | 1.28 | |
| Film Temperature Rise with Hot Channel Factor, C | 55.77 | |
| Clad Surface Temperature with All Hot Channel Factors, C | 122.5 | 122.5 |
| | | |
| Random Hot Channel Factor on Heat Flux | 1.23 | |
| Heat Flux with Hot Channel Factors, $MW/m^2$ | 0.4779 | |
| ΔTsaturation based on Bergles and Rohsenow, C | 7.41 | |
| Surface Temperature For Onset of Nucleate Boiling, C | 122.6 | 122.6 |

```
! Rhode Island, equilibrium core, 1 internal plate (LEU)
RINSC, 88 mil channel, 1 internal plate; 1580 gpm                                0100
   1   0   8   1   0       1   0   0   0   0   0   0   2   1   1   0   0   00200
         1.          1.         1.2                                          0201
   4      7.5e-3      3.0e-1   1         1.0                                  0203
   1   3          0.          1.          1.          1.   0   0             30300-1
        1.24       1.28        1.23                                         0300A-1
   1   2          1.                                                        0301-1
   1   1   1                                                                0302-1
     1.32483                                                                0303-1
         1.          1.          0.          0.                             0304-1
         1.          1.     0.59055          0.    0.066548   0.0022352      0304-1
         1.          1.          0.          0.                             0304-1
         0.          0.          0.                                         0305-1
! channel length (fueled portion)=23.25"=0.59055 m, total width=2.62"=0.066548 m,
!   and thickness=0.088"=0.0022352 m
! plate fueled width=2.395"
! channel unfueled width (each side)=(2.62"-2.395")/2=0.1125"=2.8575e-3 m
! clad thickness =0.015"=3.81e-4 m; meat thickness=0.020"=5.08e-4 m
   2   3   2.8575e-3     0.59055     3.81e-4          0.     5.08e-4         40.0306-1
! Assume thickness=0.088"; 1/2 channel on each side of plate
    7.435e-5    4.325e-3      0.0688          0.    0.066548   0.0022352      0307-1
    7.435e-5    4.325e-3      0.0688          0.    0.066548   0.0022352      0307-1
   0.0665488                                                                0308-1
         1.                                                                 0309-1
! 1580 gpm (115 F)
     0.11050     0.11050                                                    0310-1
        0.17          0.        0.17        0.01       46.11          0.     0500
         0.          0.                                                     0500
   0     0.0001        32.5          0.          0.                         0600
! Equilibrium Core, Assembly D6, Plate 1
 -18                                                                        0700
     0.00000     0.00536     0.56185                                        0701
     0.01071     0.03928     0.48115                                        0701
     0.06786     0.09643     0.52769                                        0701
     0.12500     0.15625     0.62614                                        0701
     0.18750     0.21875     0.74583                                        0701
     0.25000     0.28125     0.84137                                        0701
     0.31250     0.34375     0.95889                                        0701
     0.37500     0.40625     1.07059                                        0701
     0.43750     0.46875     1.17284                                        0701
     0.50000     0.53125     1.25813                                        0701
     0.56250     0.59375     1.31201                                        0701
     0.62500     0.65625     1.32483                                        0701
     0.68750     0.71875     1.28940                                        0701
     0.75000     0.78125     1.24832                                        0701
     0.81250     0.84375     1.12725                                        0701
     0.87500     0.90625     1.00578                                        0701
     0.93750     0.96875     0.99993                                        0701
     1.00000                                                                0701
   0                                                                        0702
```

**Figure 4.6-7 – PLTEMP/ANL V4.0 Input for Onset of Nucleate Boiling Predictions at 1580 gpm**

The coolant properties for the hand calculation were obtained from the 1996 NIST/ASME Steam Tables. The Nusselt number is based on the Dittus-Boelter correlation, i.e., $Nu = 0.023\ Re^{0.8}\ Pr^{0.4}$. The power input values to the middle and exit of node 13 were obtained with the aid of a separate spreadsheet calculation that provided the plate power for each axial level. As Table 4.6-9 shows, the clad surface temperature at the limiting location predicted in both calculations is 122.5° C and the onset of nucleate boiling is predicted in both calculations to occur at 122.6° C. The 0.1° C difference between the two values is considered to sufficiently small as to not require additional iterations of the code. The close agreement between the hand-calculation and code predictions for these two key temperatures demonstrates that the code has predicted them properly.

The PLTEMP/ANL predicted power for the onset of flow instability uses the following formula:

$$R = \frac{1}{1 + \eta/(L_H/D_H)} \tag{9}$$

where R is the ratio of the bulk coolant temperature rise from the inlet to the outlet at the onset of flow instability to the bulk to coolant temperature rise from the inlet to the coolant saturation temperature at the outlet pressure, η is taken to be 32.5, and $L_H$ and $D_H$ are the heated length and heated diameter, respectively. The heated diameter is 4 times the flow area divided by the heated perimeter. The formula was obtained from Whittle and Forgan.[15] The value of 32.5 for η was selected because a statistical analysis of the 74 experiments with rectangular channels by Whittle and Forgan[15] showed that this value is sufficient to provide 95% probability with at least a 95% confidence that flow instability would not occur.[16] Equation (9) allows the bulk coolant at the exit of the channel that corresponds to the onset of flow instability to be determined.

**Table 4.6-10 – Verification of PLTEMP/ANL Onset of Flow Instability Prediction for a Core Flow Rate of 1580 gpm**

| Quantity | Hand Calculation | PLTEMP |
|---|---|---|
| **Channel Dimensions** | | |
| **Thickness, in** | **0.088** | |
| **Width, in** | **2.62** | |
| **Heated Length, in** | **23.25** | |
| **Heat Width, in** | **2.395** | |
| | | |
| **Flow Area, $in^2$** | **0.2306** | |
| **Heated Perimeter, in** | **4.79** | |
| **Heated Diameter, in** | **0.1925** | |
| **η** | **32.5** | |
| **$R = 1/(1 + \eta/(L_H/D_H)$** | **0.7879** | |
| **Inlet Temperature (Tin), C** | **46.11** | |
| **Pressure, bar** | **1.7** | |
| **Saturation Temperature (Tsat), C** | **115.15** | |
| **Random Hot Channel Factor on Bulk ΔT** | **1.24** | |
| **(Tsat − Tin), C** | **69.04** | |
| **R × (Tsat − Tin), C** | **54.40** | |
| **R × (Tsat − Tin) / (Random Hot Channel Factor on Bulk ΔT), C** | **43.87** | |
| **Exit Temperature at Onset of Flow Instability, C** | **89.98** | |
| **Enthalpy at Inlet Temperature, kJ/kg** | **193.21** | |
| **Enthalpy at Onset of Flow Instability Exit Temperature, kJ/kg** | **377.03** | |
| **Power at Onset of Flow Instability, kW** | **40.62** | **40.72** |

Key results for the hand calculation of the power at which the onset of flow instability is predicted to occur are shown in Table 4.6-10. The allowed bulk coolant temperature rise from the inlet to the exit that is obtained with the aid of equation (9) is divided by the random hot channel factor for the bulk coolant temperature rise, 1.24. The result is added to the inlet temperature to obtain the allowed exit coolant temperature. For this temperature and the specified pressure of 1.7 bar the 1996 NIST/ASME Steam Table provide the corresponding exit coolant enthalpy. The coolant enthalpy at the inlet is obtained from the inlet temperature of

46.11° C and 1.7 bar pressure in a similar manner. The product of the channel coolant flow rate and the enthalpy rise from the inlet to the outlet provides the allowed channel power at the onset of flow instability, which is 40.62 kW. The PLTEMP/ANL code has a search capability that adjusts the channel power until the onset of flow instability is predicted. PLTEMP/ANL predicted the onset of flow instability to occur at 40.72 kW, which is within only 0.3% of that predicted by the hand calculation. Thus, this comparison demonstrates the PLTEMP/ANL is predicting the onset of flow instability properly. The PLTEMP/ANL V4.0 input listing that was used to produce the flow instability prediction is the same as that list in Figure 4.6-7 with one exception – the number 4 at the start of the fifth line (Card 203 in the code) should be replaced with a number 7.

### 4.6.10 Results of Steady-State Thermal Analysis

Table 4.6-11 summarizes the onset of nucleate boiling results of the thermal analysis. First, the hydraulics model presented above was used to determine the flow rate in the limiting channel as a function of flow rate through the reactor flow meter. The limiting channel for the analysis is one that is between two fuel plates of the same fuel assembly. Thus, when the reactor is running at the minimum flow rate allowed by the technical specifications for forced convection, 1580 gpm, the flow rate in the limiting channel is 0.2210 kg/s. In the PLTEMP/ANL model, half of the 0.2210 kg/s is assumed to flow in each of the two half channels, each with the flow area of half of a channel but the hydraulic diameter of a whole channel. The PLTEMP/ANL analysis shows that onset of nucleate boiling occurs when the power in the plate between the two half channels is at 22.80 kW. The analysis of the power distribution in the equilibrium core shows that when the reactor is operating at 2.0 MW, the power in the limiting plate is 9.653 kW. Thus, 22.80 kW corresponds to reactor operation at 4.72 MW, i.e., 22.80/9.653 × 2.0 MW = 4.72 MW. Similarly, in Table 4.6-12 the PLTEMP/ANL analysis predicts for a reactor flow of 1580 gpm the onset of flow instability to occur in the limiting channel at a channel power of 40.72 kW, which corresponds to a reactor power of 8.44 MW.

**Table 4.6-11 – Summary of Steady-State Onset of Nucleate Boiling Results**

| Limiting Channel | | Reactor | |
|---|---|---|---|
| Flow, kg/s | ONB Power, kW | Flow, gpm (120° F Water) | ONB Power, MW |
| 0.1395 | 15.13 | 1000 | 3.13 |
| 0.1676 | 17.82 | 1200 | 3.69 |
| 0.1957 | 20.46 | 1400 | 4.24 |
| 0.2210 | 22.80 | 1580 | 4.72 |
| 0.2238 | 23.05 | 1600 | 4.78 |
| 0.2520 | 25.63 | 1800 | 5.31 |
| 0.2801 | 28.16 | 2000 | 5.83 |
| 0.3083 | 30.67 | 2200 | 6.35 |

The power at which critical heat flux, or departure from nucleate boiling, as it is also called, was also predicted. The correlation of Sudo and Kaminaga[17,18] was used for predicting the critical heat flux. It was selected because it is a more recent correlation, having been developed in the 1990s, that is specifically for thin rectangular channels in research reactors. The minimum channel thickness covered by the correlation is 2.25 mm (0.0886 inches). The channel thickness in RINSC fuel elements is 0.0880 inches. The correlation includes two-sided heating and downward flow.

**Table 4.6-12 – Summary of Steady-State Flow Instability and Critical Heat Flux Results**

| Limiting Channel | | | | Reactor | | | |
|---|---|---|---|---|---|---|---|
| Flow, kg/s | Power, kW | | | Flow, gpm (120° F Water) | Power, MW | | |
| | Whittle & Forgan Flow Instability | Sudo & Kaminaga CHF Correlation | Mirshak et al. CHF | | Whittle & Forgan Flow Instability | Sudo & Kaminaga CHF Correlation | Mirshak et al. CHF |
| 0.1395 | 25.70 | 24.9 | 98.7 | 1000 | 5.32 | 5.16 | 20.4 |
| 0.1676 | 30.88 | 29.9 | 101 | 1200 | 6.40 | 6.20 | 20.9 |
| 0.1957 | 36.06 | 34.9 | 103 | 1400 | 7.47 | 7.24 | 21.3 |
| 0.2210 | 40.72 | 39.4 | 104 | 1580 | 8.44 | 8.17 | 21.6 |
| 0.2238 | 41.24 | 39.9 | 105 | 1600 | 8.54 | 8.28 | 21.7 |
| 0.2520 | 46.43 | 45.0 | 107 | 1800 | 9.62 | 9.32 | 22.1 |
| 0.2801 | 51.61 | 50.0 | 109 | 2000 | 10.69 | 10.36 | 22.5 |
| 0.3083 | 56.81 | 55.0 | 111 | 2200 | 11.77 | 11.40 | 23.0 |

In the past the Mirshak et al. correlation, which was published in 1959 and developed for thin rectangular and thin annular channels, has been used to predict critical heat flux in many MTR-type research reactors. The Mirshak correlation is based on 65 experiments with downward flow and one-sided heating. The minimum hydraulic diameter among these 65 experiments is larger than the 4.325 mm (0.170 inches), Table 4.6-5, being considered for the RINSC reactor. For comparative purposes predictions made with the Mirshak et al. correlation are provide along with the predictions made with the Sudo and Kaminaga correlation. Table 4.6-12 provides both the Sudo and Kaminaga and the Mirshak et al. critical heat flux results along side the Whittle and Forgan flow instability results.

Four separate sets of PLTEMP/ANL analyses – one for onset of nucleate boiling, one for flow instability, and two for critical heat flux – were performed for each of the eight limiting channel flow rates shown in the Tables 4.6-10 and 4.6-11. Each analysis included the hot channel factors and used the maximum allowable core inlet temperature and the minimum water depth as prescribed by the reactor Technical Specifications. The onset of nucleate boiling, flow instability, and Sudo and Kaminaga critical heat flux results for the reactor, as provided on the right sides of Tables 4.6-10 and 4.6-11 are plotted in Figure 4.6-8.

### 4.6.11 Discussion

As Figure 4.6-8 shows, the Sudo and Kaminaga critical heat flux results predict that critical heat flux occurs at 97% of the power that produces flow instability. This ratio is either 0.968 or 0.969 for all eight flow rates in Tables 4.6-10 and 4.6-11. However, critical heat flux may not occur before flow instability in the RINSC reactor. The reason that the Sudo and Kaminaga correlation predicts critical heat flux to precede flow instability may be that some of the Sudo and Kaminaga experimental data do not distinguish between critical heat flux that is not caused by flow instability and that which is. This is indicated in the second column on page 429 of Reference 18. Thus, the close agreement between the flow instability and critical heat flux predictions is likely to be another confirmation of the flow instability predictions and a lower bound for critical

heat flux. Therefore, the steady-state thermal-hydraulics margin in the RINSC reactor will be based on the Sudo and Kaminaga correlation results. For completeness the Mirshak et al. predictions of critical heat flux are also included, are shown in Table 4.6-12.

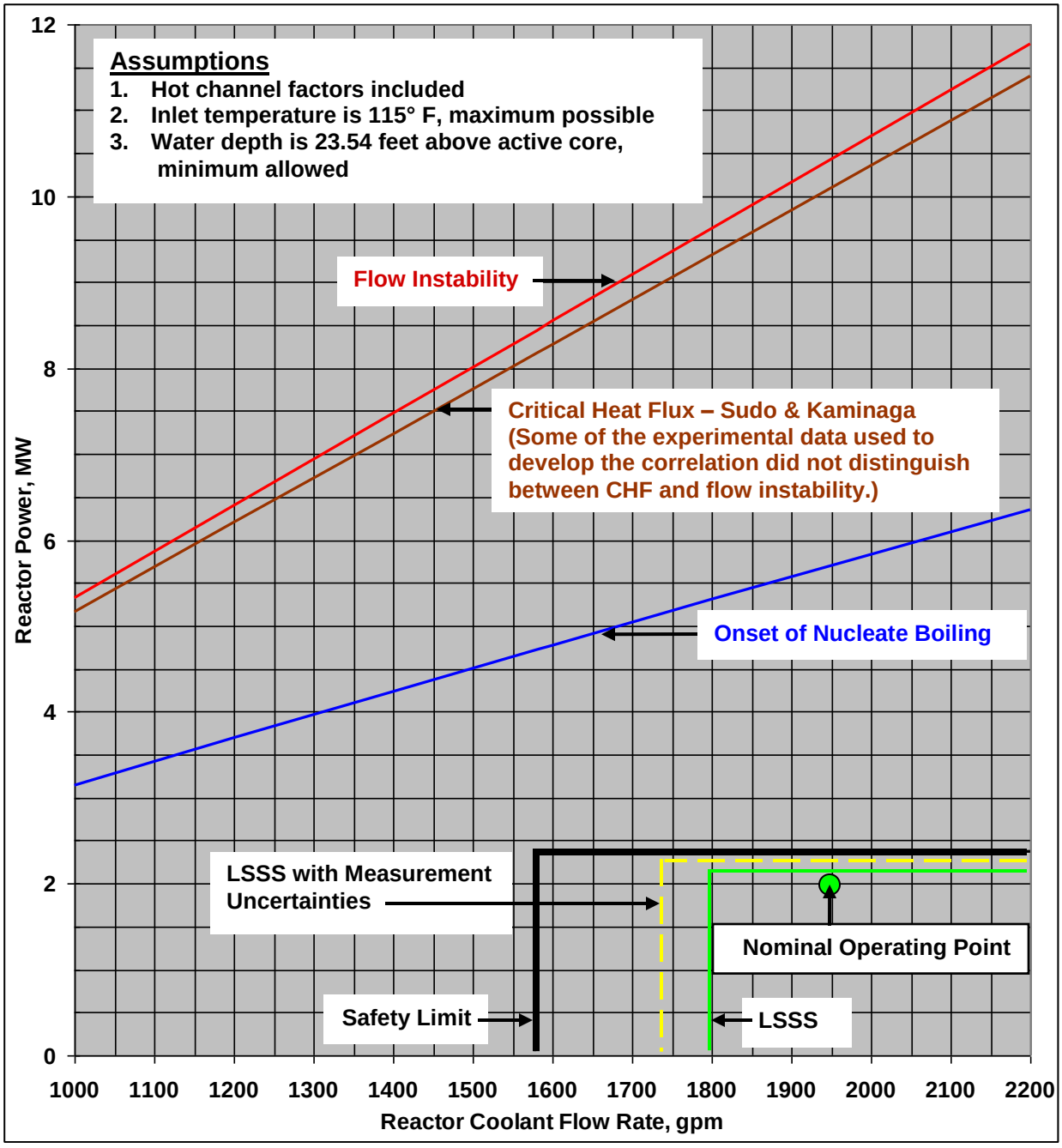


**Figure 4.6-8 – Reactor Powers at Which Onset of Nucleate Boiling, Critical Heat Flux, and Flow Instability are Predicted to Occur**

Manufacturing tolerances and Nusselt number correlation uncertainties were included in the hot channel factor analysis presented above. The Bergles and Rohsenow correlation predicts that onset of nucleate boiling occurs when the clad surface temperature is only several degrees

Celsius above the saturation temperature. For example, for the limiting channel when the reactor flow is at the safety limit value of 1580 gpm, this temperature rise is only 7.4° C, (See Table 4.6-9.) and the total temperature rise from the reactor inlet to the clad surface temperature at the onset of nucleate boiling is 122.5 − 46.1° C (See Table 4.6-9.), or 76.4° C. Thus, a small uncertainty in the 7.4° C Bergles and Rohsenow temperature rise would correspond to only a very small relative error in the power at which the onset of nucleate boiling is predicted to occur and is neglected in the current analysis. The uncertainty in the flow instability correlation is taken into account via the parameter η in equation (9).

In the PLTEMP/ANL calculations that produced the power predictions in the Tables 4.6-10 and 4.6-11 no consideration was given to measurement errors in reactor power or reactor flow rate. Thus, the results plotted in Figure 4.6-8 correspond to true reactor powers and true reactor flow rates. Measurement errors are included in the interpretation of the figure. In the Technical Specifications, the safety limits for power operation with forced convection are 1580 gpm and 2.4 MW. These are indicated by the heavy solid black lines in the figure. The nominal operating point for the reactor is 1950 gpm and 2.0 MW, as indicated by the light green circle. The Limiting Safety Systems Settings (LSSS) for forced convection are 1800 gpm and 2.1 MW, which are measured quantities. These are indicated by the solid light green lines in Figure 4.6-8. The flow meter has a measurement uncertainty of ±60 gpm. The power has a measurement uncertainty of ±0.2 MW. When these uncertainties in measurement are taken into account, at the LSSS the true flow rate could be as low as 1740 gpm and the true power level could be as high as 2.3 MW, as indicated by the dashed yellow lines in the figure. These limiting true LSSS values leave a 160 gpm margin to the safety limit flow rate and a 0.1 MW margin to the safety limit power.

The onset of nucleate boiling will not result in fuel damage and is therefore not considered to be a safety limiting event. While flow instability or critical heat flux can cause fuel damage, neither can occur unless nucleate boiling occurs. As the Figure 4.6-8 and Tables 4.6-10 and 4.6-11 show, if the true reactor flow rate is at its minimum value of 1580 gpm, then onset of nucleate boiling is predicted to occur at 4.72 MW, onset of critical heat flux using the Sudo and Kaminaga correlation is predicted to occur at 8.17 MW, and onset of flow instability based on the Whittle and Forgan correlation is predicted to occur at 8.44 MW. Since the maximum allowed true reactor power is 2.4 MW, for any of the allowed forced-convection steady-state conditions the predicted margins to onset of nucleate boiling, critical heat flux, and flow instability are 2.32, 5.77, and 6.04 MW, respectively, at the safety limiting flow rate and higher at all higher flow rates. Thus, the predicted thermal margin to fuel damage is a factor of 3.4, i.e., 8.17/2.4 = 3.4, at the safety limiting flow rate and higher for higher flow rates.

### 4.6.12 Summary and Conclusions

The steady-state thermal analysis of the RINSC reactor operating under forced-flow conditions has been analyzed using the PLTEMP/ANL V4.0 code. Reactor flow rates ranging from 1000 to 2200 gpm were considered in the analysis. A separate hydraulics model was developed from engineering fundamentals and used to predict the flow rate in each fueled reactor channel over the specified range of reactor flow rates. The coolant inlet temperature and pool water depth

were assumed to be at their extreme values from a safety perspective – maximum for inlet temperature and minimum for water depth.

The equations used in the hydraulics model are provided above. For the safety limiting reactor flow rate of 1580 gpm, specific hydraulic results are provided in tabular form so that one can verify that the models were implemented correctly. For this flow rate the PLTEMP/ANL V4.0 code predictions of the power at which onset of nucleate boiling and the power at which the onset of flow instability occurs were checked by hand calculations. The specific results from these calculations are also provided in tables as an important form of verification.

For each of eight specific reactor flow rates, the PLTEMP/ANL code was used to predict the following four quantities: 1) the power at which the onset of nucleate boiling is predicted to occur, based on the Bergles and Rohsenow correlation,[14] 2) the onset of flow instability, based on the Whittle and Forgan correlation,[15] 3) the onset of critical heat flux, based on the Sudo and Kaminaga correlation,[17,18] and 4) the onset of critical heat flux, based on the Mirshak et al. correlation.[19] The results are shown in Tables 4.6-10 and 4.6-11 and Figure 4.6-8. The Sudo and Kaminaga correlation predicts critical heat flux to occur at 97% of the power that flow instability is predicted to occur. This may be due to some of the Sudo and Kaminaga experimental data not distinguishing between the two phenomena. The Mirshak et al. correlation predictions are not plotted in Figure 4.6-8 because it predicts critical heat flux to occur at power levels that are 2 to 4 times as great as those predicted by the Sudo and Kaminaga correlation and also about 2 to 4 times those predicted by the Whittle and Forgan flow instability correlation.

As Figure 4.6-8 shows, the safety margins are smallest at the safety limiting flow of 1580 gpm and increase steadily with reactor flow rate. At this limiting flow rate the onset of nucleate boiling is predicted to occur at 4.72 MW, which is 2.32 MW above the safety limit power of 2.4 MW. However, onset of nucleate boiling is a precursor to flow instability and critical heat flux (also called departure from nucleate boiling), either of which can cause fuel damage. Based on the Sudo and Kaminaga correlation, at 1580 gpm the critical heat flux is predicted to occur at 8.17 MW, which leaves a safety margin of 5.77 MW to the safety limiting power, or a factor of 3.4. At 1580 gpm flow instability is predicted to occur at 8.44 MW, which leaves a safety margin of 6.04 to the safety limiting power, or a factor of 3.5. Since either critical heat flux or flow instability can cause fuel damage, the safety margin is 3.4 at the minimum flow of 1580 gpm and higher at all other allowed flows.

**References:**


1. B. J. Tharpe, *Safeguards Report for the Rhode Island Open Pool Reactor*, APED-3872, Class II, General Electric Co., San Jose, California, April 4, 1962.
2. I. E. Idelchik, *Handbook of Hydraulic Resistance*, Second Edition, Hemisphere Publishing Corporation, New York, 1986, pp. 149-151.
3. Operation and Maintenance Manual, One-Megawatt Open Pool Reactor for Rhode Island Atomic Energy Commission, Providence, RI, GEI-77793, General Electric, San Jose, California, October 1962.

4. Arne P. Olson and Kalimullah, "A Users Guide to the PLTEMP/ANL V4.0 Code," Global Threat Reduction Initiative (GTRI) – Conversion Program, Nuclear Engineering Division, Argonne National Laboratory, March 24, 2010.
5. K. Mishima, K. Kanda and T. Shibata, "Thermal-Hydraulic Analysis for Core Conversion to the Use of Low-enrichment Uranium Fuels in the KUR," KURRI-TR-258, Research Reactor Institute, Kyoto University, Dec. 7, 1984.
6. K. Mishima, K. Kanda and T. Shibata, "Thermal-Hydraulic Analysis for Core Conversion to the Use of Low-Enriched Uranium Fuels in the KUR," ANL/RERTR/TM-6, CONF-8410173, p. 375, 1984.
7. W. L. Woodruff and K. Mishima, "Neutronics and Thermal-Hydraulics Analysis of KUHFR," ANL/RERTR/TM-3, CONF-801144, p. 579, 1980.
8. W. L. Woodruff, "Some Neutronics and Thermal-hydraulics Codes for Reactor Analysis Using Personal Computers," Proc. Int. Mtg. on Reduced Enrichment for Research and Test Reactors, Newport, RI, Sept. 23-27, 1990, CONF-9009108 (ANL/RERTR/TM-18), Argonne National Laboratory (1993).
9. W. L. Woodruff, J. R. Deen and C. Papastergiou, "Transient Analyses and Thermal-hydraulic Safety Margins for the Greek Research Reactor (GRR1)," Proc. Int. Mtg. on Reduced Enrichment for Research and Test Reactors, Williamsburg, VA, Sept. 19-23, 1994, CONF-9409107 (ANL/RERTR/TM-20), Argonne National Laboratory (1997).
10. W. L. Woodruff, "A Kinetics and Thermal-hydraulics Capability for the Analysis of Research Reactors," Nucl. Technol., Volume 64, 196 (1983).
11. W. L. Woodruff and R. S. Smith, "A Users Guide for the ANL Version of the PARET Code, PARET/ANL (2001 Rev.)," ANL/RERTR/TM-16, Mar. 2001.
12. TRTR-6 Specification Test Research Training Reactor LEU Silicide U3Si2 Fuel Plates, Revision 4, May 20, 1988, EG&G Idaho, Inc.
13. W. L. Woodruff, *Evaluation and Selection of Hot Channel (Peaking) Factors for Research Reactor Applications*, ANL/RERTR/TM-28, RERTR Program, Argonne National Laboratory, Argonne, Illinois, February 1997 [http://www.rertr.anl.gov/METHODS/TM28.pdf].
14. A. E. Bergles and W. M. Rohsenow, "Determination of Forced-Convection Surface-Boiling Heat Transfer," Trans. ASME, J. Heat Transfer 86, pp. 365-372, (1964).
15. R. H. Whittle and R. Forgan, "A Correlation for the Minima in the Pressure Drop Versus Flow-Rate Curves for Sub-Cooled Water Flowing in Narrow Heated Channels," *Nuclear Engineering and Design*, 1967, pp. 89-99.
16. A. P. Olson, "Analysis of Flow Excursion Experiments Relevant to Research Reactors," The 2006 International Meeting on Reduced Enrichment for Research and Test Reactors, October 29-November 3, 2006, Cape Town, South Africa, http://www.rertr.anl.gov/RERTR28/PDF/S7-2_Olson.pdf.
17. Masanori Kaminaga, Kazuyoshi Yamamoto, and Yukio Sudo, "Improvement of Critical Heat Flux Correlation for Research Reactors Using Plate-Type Fuel," *Journal of Nuclear Science and Technology*, Vol 35, No. 12, pp. 943-951 (December 1998).
18. Y. Sudo and M. Kaminaga, "A New CHF Correlation Scheme Proposed for Vertical Rectangular Channels Heated From Both Sides in Nuclear Research Reactors," *Transactions of the ASME, Journal of Heat Transfer*, Vol. 115, May 1993, pp. 426-434.

19. S. Mirshak, W. S. Durant, and R. H. Towell, *Heat Flux at Burnout*, AEC Research and Development Report, DP-355, E. I. du Pont de Memours & Co., Savannah River Laboratory, Aiken, South Carolina, February 1959.